ISSN 1029-9599, Physical Mesomechanics, 2023, Vol. 26, No. 4, pp. 367–390. © Pleiades Publishing, Ltd., 2023.
Russian Text © The Author(s), 2023, published in Fizicheskaya Mezomekhanika, 2023, Vol. 26, No. 2, pp. 5–29.

Fatigue and Fracture Behavior of AlSi10Mg Manufactured by Selective Laser Melting: A Review

Z. Jiang[1], J. Sun[2], F. Berto[3,4], X. Wang[1]*, and G. Qian[2]**

[1] *School of Mechanical, Electronic and Control Engineering, Beijing Jiaotong University, Beijing, 100044 China*
[2] *State Key Laboratory of Nonlinear Mechanics, Institute of Mechanics, Chinese Academy of Sciences, Beijing, 100190 China*
[3] *Department of Mechanical and Industrial Engineering, Norwegian University of Science and Technology, Trondheim, 7491 Norway*
[4] *Department of Chemical Engineering Materials Environment, Sapienza University of Rome, Rome, 00184 Italy*
** e-mail: wangxi@bjtu.edu.cn*
*** e-mail: qianguian@imech.ac.cn*

Received May 23, 2022; revised September 30, 2022; accepted December 4, 2022

Abstract—Selective laser melting (SLM) is one of the most promising metal additive manufacturing technologies. SLMed Al-Si alloys have been widely used in the rail transport, aerospace, and automotive industries. Recently, the fatigue and fracture properties of SLMed Al-Si alloys have attracted considerable attention due to their application in critical load-bearing structures. This review aims to better understand the recent progress on the fatigue and fracture investigations of SLMed Al-Si alloys, especially AlSi10Mg, with emphasis on the effect of defects, heterogeneous microstructure, residual stress, and post-treatment methods. In addition, fatigue and fracture modeling methods are discussed. Finally, the challenges and future research opportunities are prospected.

Keywords: selective laser melting, AlSi10Mg, crack initiation, post-treatment, fatigue life prediction
DOI: 10.1134/S102995992304001X

1. INTRODUCTION

Additive manufacturing is regarded as a major component of Industry 4.0. In the past decade, significant progress has been made in processing metallic parts by this method. Among metal additive manufacturing technologies, selective laser melting has attracted widespread attention [1]. During the SLM processing, laser beams serve as the energy source, and metal parts are formed by melting metal powder layer by layer based on computer-aided design models. This technology makes it possible to fabricate custom structures with complex geometries and high mechanical properties that are difficult to process using conventional manufacturing technologies such as casting and forging [2–6]. Consequently, SLM provides a powerful tool for the fabrication of lightweight structures for the automotive, aerospace, and rail transport industries.

Al-alloys are in high demand for additive manufacturing as they have an excellent compromise between strength and density [7, 8]. However, they are considered challenging when processed by SLM because of high reflectivity, high thermal conductivity, and low laser absorptivity [9]. In recent years, Al-Si alloys, especially AlSi10Mg, have received the most attention among SLMed Al-alloys. The low melting point, narrower solidification temperature range, and low hot tearing susceptibility make them suitable for SLM. On the contrary, many wrought Al-alloys are difficult to process by SLM due to their strong tendency to crack. In recent years, with the development of SLM, there has been some success in processing these types of alloys, such as Al 7075 + Zr [10, 11], Al-Mn-Sc [12, 13], and nano-TiB_2 decorated AlSi10Mg [14, 15]. Since SLMed AlSi10Mg presents the highest maturity among SLMed Al-alloys, this review mainly focuses on this alloy.

Fatigue and fracture are the most common failure modes of load-bearing structures. Although SLM has many advantages, it still requires strict structural integrity certification before it can be used for load-bearing components [16]. Figure 1 summarizes the parameters affecting the fatigue and fracture properties of SLMed alloys. The defects, heterogeneous microstructures, and high residual stresses are three dominating factors [17, 18]. Due to the layer-by-

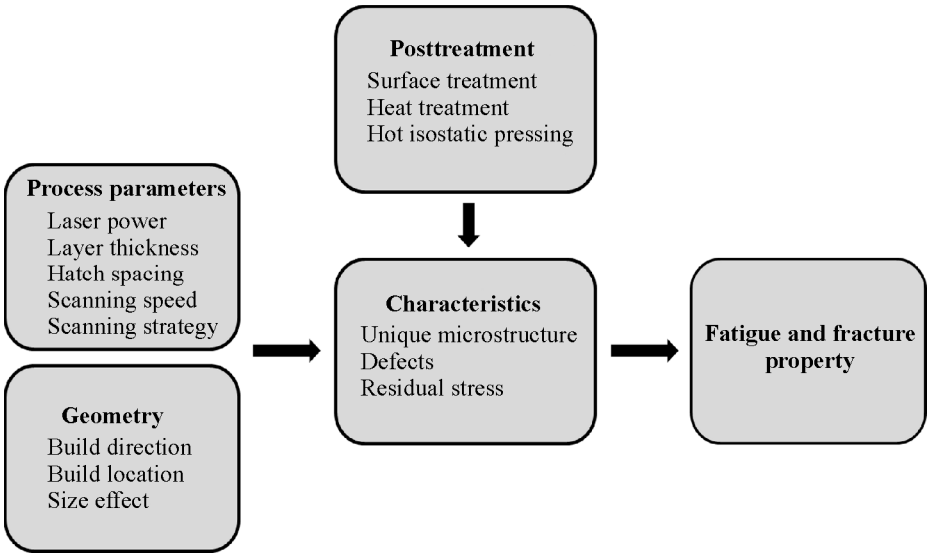

Fig. 1. The parameters affecting the fatigue and fracture performance of SLMed AlSi10Mg.

layer processing, pores, lack of fusion defects, and large surface roughness are inevitably formed in the SLMed structures. When the structures are subjected to fatigue loading, these defects act as potential sites of fatigue crack initiation and result in fatigue life dispersion [19, 20]. Poor mechanical properties of conventional cast Al-alloy components stem from their coarse-grained microstructure formed due to low cooling rate. SLMed AlSi10Mg has a more refined microstructure as a result of very high cooling rate and therefore higher mechanical properties [21, 22]. Another advantage of SLM, similar to the welding process, is the formation of the melt pool during laser melting. However, a complex residual stress state induced by the SLM process increases the complexity of fatigue and fracture behaviors [23]. These factors are determined by varying process parameters, structure geometry, and posttreatment methods. With the change of processing parameters (laser power, scanning speed, layer thickness, hatch spacing, etc.) or geometry information (build direction, build location, geometry size, etc.), the thermal history changes significantly and results in different microstructural features [24]. Appropriate postprocessing methods for SLMed alloys, including surface treatment methods [25–28], heat treatment schedules [29–32] and hot isostatic pressing [33–37], are regarded as effective ways to enhance the fatigue and fracture properties. These procedures are highly recommended before SLMed parts are used in engineering applications.

In recent years, the review papers related to SLMed Al-alloys have focused on process optimization, microstructure characteristics, and tensile properties [7–9, 38, 39]. However, there is still a lack of a detailed overview on the fatigue and fracture properties. This review aims to summarize state-of-the-art studies on the fatigue and fracture of SLMed AlSi10Mg and discuss the application of this alloy in load-bearing structures.

2. THE CHARACTERISTICS OF SLMED AlSi10Mg

2.1. Microstructure

The literature contains many reports on the multiscale microstructure of SLMed Al-Si alloys [21, 22, 40–45]. The typical microstructure of SLMed AlSi10Mg is shown in Fig. 2, where the build direction (B.D.) of the samples is marked with arrows. A 3D optical microscopy image of SLMed AlSi10Mg is shown in Fig. 2a. Fish-scale melt pools can be clearly observed on the *xOz* and *yOz* planes [44]. Strip-like patterns along various laser scanning directions, determined by the scanning strategy, can be seen on the *xOy* plane [45]. Figure 2b shows a scanning electron microscopy image of the microstructure near the melt pool boundary. SLMed AlSi10Mg is composed of an α-Al phase and a Si-rich eutectic phase, and the α-Al matrix is surrounded by a Si precipitate network. The microstructure near the melt pool boundary is not homogenous, and there are three different regions according to the morphology of the Si precipitates: fine-grained, coarse-grained, and heat-affected zone (HAZ). Si precipitates are well interconnected in the fine- and coarse-grained

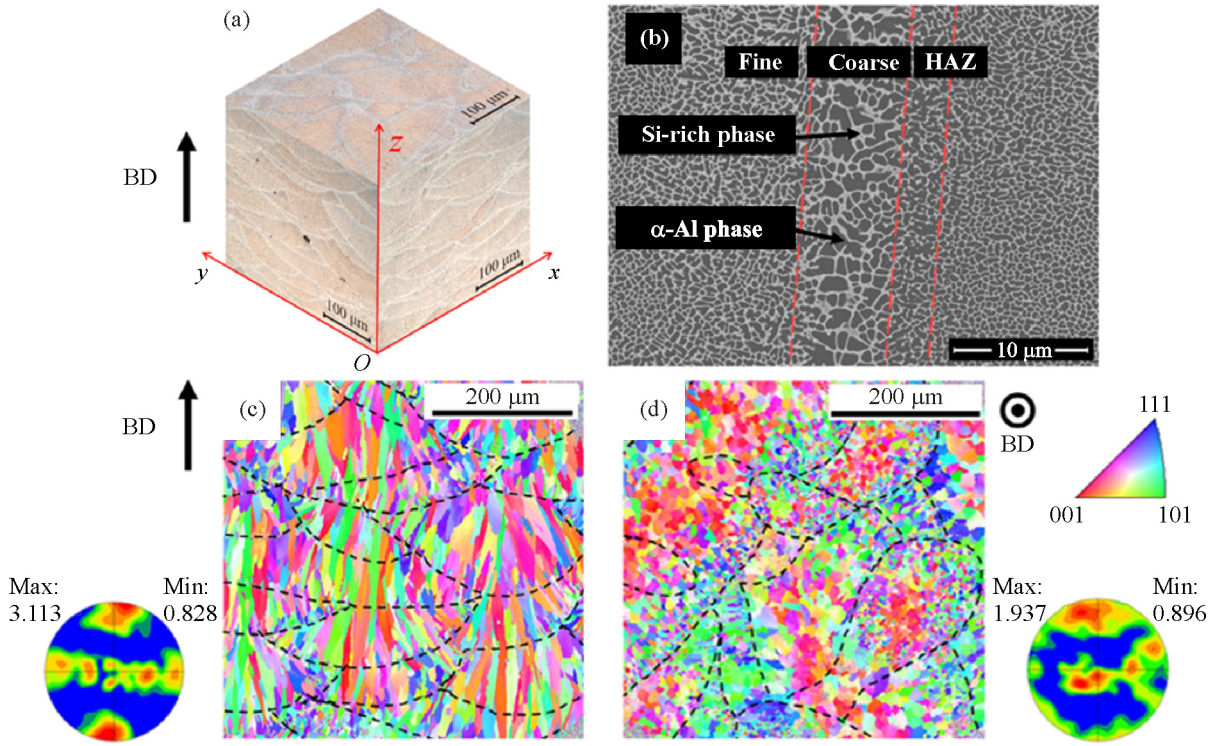

Fig. 2. 3D optical microscopy image of SLMed AlSi10Mg [44] (a), microstructure near the melt pool boundary [43] (b), EBSD IPF maps (melt pool boundaries are drawn as dashed lines) [45] (c, d) (color online).

zones but disintegrate in the HAZ [43]. The morphology of the α-Al grain is depicted in EBSD IPF maps in Figs. 2c, 2d. The α-Al phase microstructure is formed primarily by columnar grains, and equiaxed grains are identified around the melt pool boundary [45].

2.2. Metallurgical Defects

In the last decade, many parameter optimization studies have been performed to find a process window to reduce metallurgical defects. As a result, the metallurgical quality of SLMed AlSi10Mg has improved significantly from the early days. However, up to now defects within the alloy cannot be eliminated [46, 47]. Figure 3 shows typical defects in SLMed AlSi10Mg samples, including lack of fusion defects and pores [48]. Inclusions were also reported by Tang et al. [49]. During the SLM processing, pores are formed due to excessive energy input or unstable gas. They are always small and highly spherical. Lack of fusion defects are caused by inadequate energy input and incomplete fusion of metal powder.

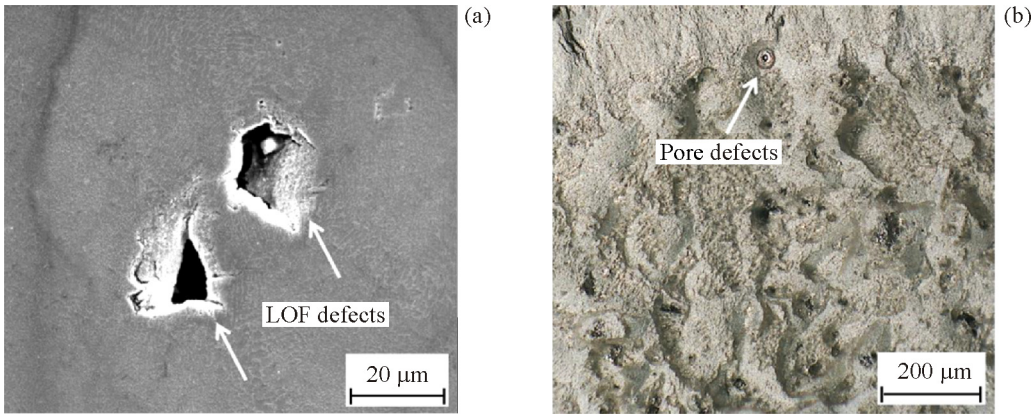

Fig. 3. Typical defects in SLMed AlSi10Mg: lack of fusion (LOF) defects (a) and pore defect [48] (b).

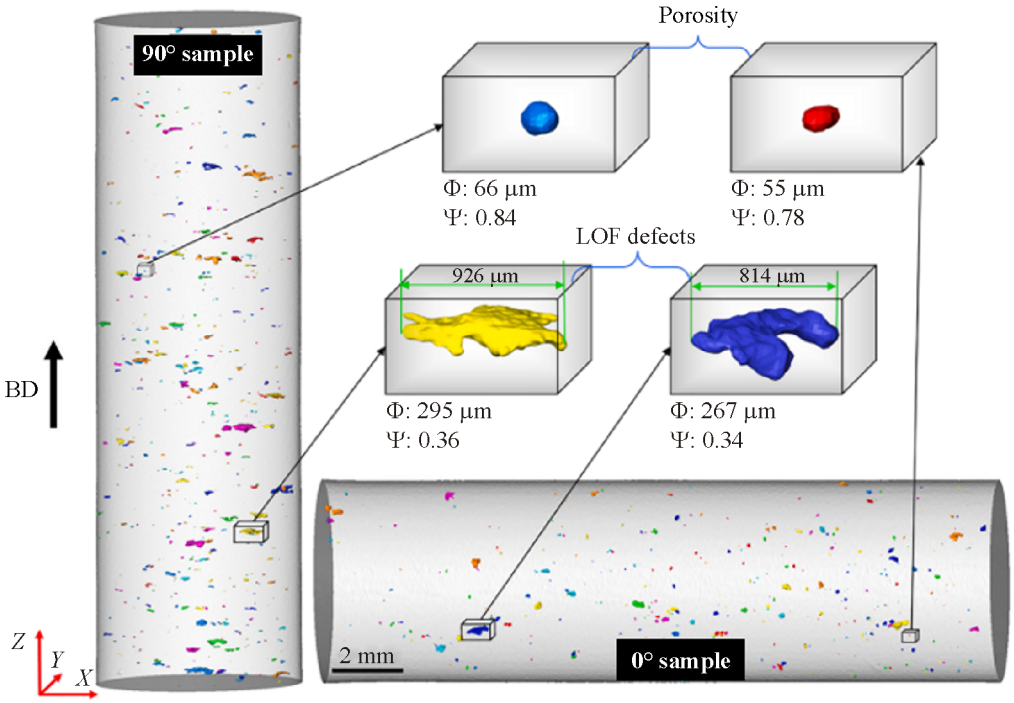

Fig. 4. 3D renderings of pores and lack of fusion defects for samples with two different build directions [52] (color online).

They always show an irregular shape and large size. Lack of fusion defects have a more harmful effect on mechanical properties than pores and inclusions [48].

Defects in SLMed alloys, on the one hand, should be minimized by optimizing process parameters or performing posttreatment, such as hot isostatic pressing. On the other hand, their effect on fatigue performance should be thoroughly explored. The internal defect size, location, and shape are essential for evaluating the fatigue properties [50–52]. A lot of defect detection methods, such as the Archimedes approach, SEM/OM observation, and X-ray computed tomography, have been used to identify the internal quality of SLM parts [53]. The Archimedes method is commonly used to measure the density and porosity of materials but cannot provide detailed information about defects. SEM/OM observation is a high accuracy method and is easy to operate. However, it is a destructive detection method and cannot provide 3D information about defects. Computed tomography is a non-destructive testing tool and allows 3D characterization of defects, including defect size, location, and distribution. It has been recognized as the most promising for SLMed alloys [51–55]. Figure 4 shows a rendering of 3D microdefects, including pores and lack of fusion defects in SLMed AlSi10Mg samples with two build directions. The equivalent diameter Φ and sphericity Ψ of the defects are given. The defect information can be useful for subsequent fatigue life predictions. It can also be used together with the finite element method to determine the actual stress distribution near defects [54]. In-situ fatigue testing can be performed in conjunction with computed tomography, which is a valuable tool for studying interactions between cracks, defects, and microstructures [51, 55]. However, the cost of computed tomography is relatively high, and the resolution is low when testing large samples.

2.3. Residual Stress

Before discussing the fatigue and fracture properties of SLMed AlSi10Mg, it is necessary to introduce the residual stress for SLMed structures [23, 56–61]. Residual stress is the stress that exists in a body at equilibrium condition when there is no external force acting on it. There are three main types of residual stress: macroscopic one, also known as the first type of residual stress, which is the average stress distributed in a macroscopic region across multiple grains. The second type of residual stress is distributed between grains or subgrains, and the third type develops within grains. The first type of residual stress is mainly considered in engineering applications.

The complex thermal history of SLMed parts experienced during processing leads to a high self-

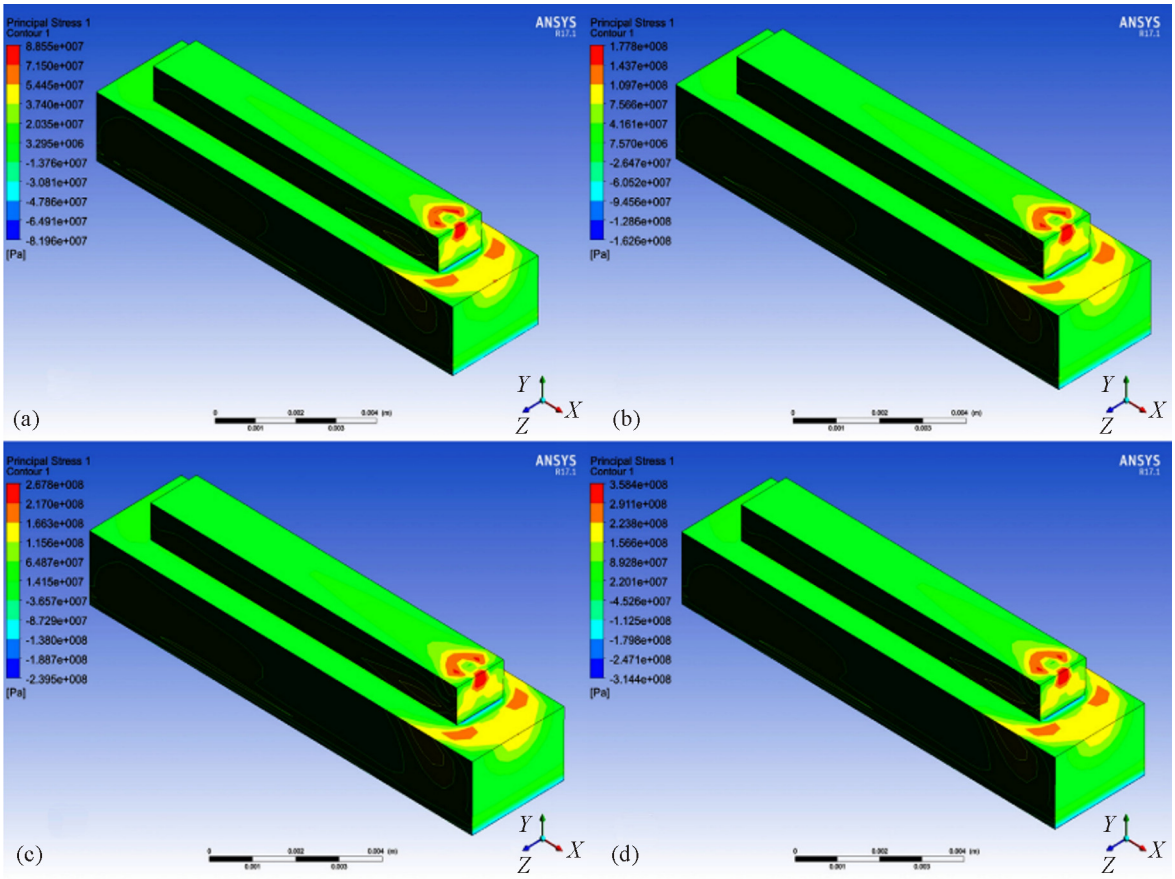

Fig. 5. Principal stress distribution at different laser powers of 50 (a), 100 (b), 150 (c) and 200 W (d) with a scanning speed of 100 mm/s [64] (color online).

equilibrating residual stress [57]. When the strength of the alloy is less than the residual stress, the part releases the residual stress through the generation and propagation of cracks. In addition, surface treatment methods can also induce compressive residual stress. Residual stresses in structures can significantly affect fatigue behaviors. Therefore, residual stresses in SLMed alloys need to be accurately characterized and predicted.

A series of experimental and numerical studies have been conducted on SLMed AlSi10Mg. For example, Salmi et al. [62] measured residual stresses in SLMed AlSi10Mg samples with and without supports using the hole-drilling method. It was found that the sample with supports shows greater residual stress than that without supports. Residual stresses can be reduced by stress relief annealing, but cannot be eliminated. Beretta et al. [63] measured residual stresses in SLMed AlSi10Mg with different build directions using X-ray diffraction. The results indicate that the residual stress distribution varies with different build directions. Panda et al. [64] established a thermo-mechanical model and studied the effect of laser power and scanning speed on residual stress distribution in SLMed AlSi10Mg parts. It was found that the residual stress increases with laser power and decreases with scanning speed (Fig. 5). Nazami et al. [65] developed a thermo-mechanical model to investigate the effect of laser spot overlap on residual stress in SLMed AlSi10Mg components. It was shown that the residual stress increases with the laser spot overlap. The experimental and simulation results can guide the optimization of process parameters. They can also be considered as the initial conditions for fatigue and fracture prediction.

3. FATIGUE AND FRACTURE PROPERTIES OF SLMED AlSi10Mg

3.1. Effect of Defects on Fatigue Crack Initiation

In contrast to failures resulting from static loading, fatigue crack initiation is a phenomenon usually caused by local stress concentration. It was widely reported that the process-induced defects signifi-

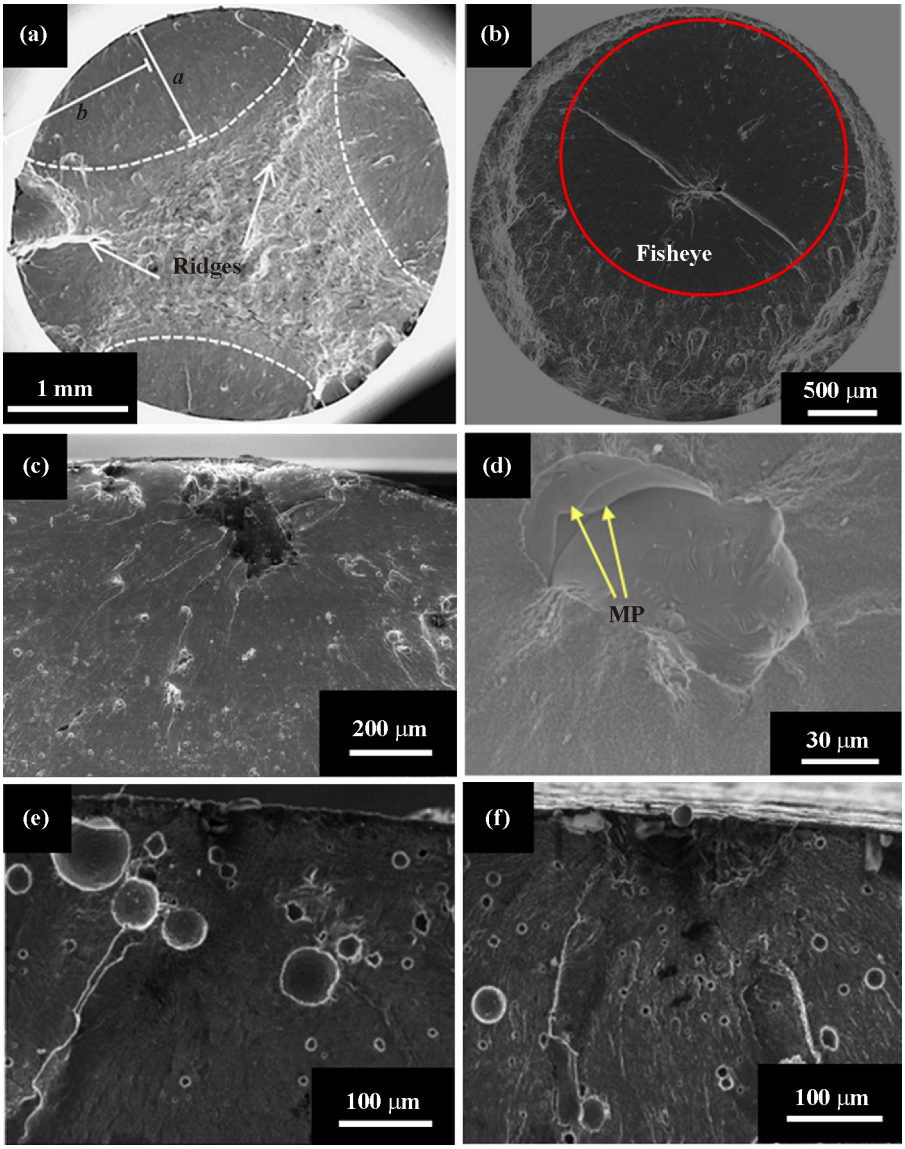

Fig. 6. Examples of crack initiation in SLMed AlSi10Mg: multipoint defects in the LCF region [44] (a), internal lack of fusion defects in the VHCF region [20] (b), subsurface lack of fusion defects [66] (c), melt pool boundary [20] (d), cluster of pores [29] (e), defects formed during the removal of support structures [29] (f).

cantly affect fatigue initiation in SLMed AlSi10Mg [29, 48, 66–68]. Figure 6 illustrates examples of crack initiation sites. As shown in Fig. 6a, in the low cycle fatigue (LCF) region, the crack tends to initiate at many points in the surface or subsurface of samples. In the high cycle fatigue (HCF) and very-high-cycle fatigue (VHCF) regions, especially the VHCF region, cracks usually initiate at internal defects (Fig. 6b). As reported in existing studies, crack initiation at lack of fusion defects appears to be the most common initiation mode (Figs. 6b, 6c). Other failure modes have also been observed, such as at the melt pool boundary (Fig. 6d) [20] or in the cluster of pores and defects originated during the removal of support structures (Figs. 6e, 6f) [29].

Lack of fusion defects in SLMed alloys are generally directional due to layer-by-layer processing. This anisotropy usually results in the anisotropy of fatigue strength [44, 52, 67]. For example, Wu et al. [52] reported that the fatigue strength of 0° SLMed AlSi10Mg samples is much higher than that of 90° samples (Fig. 7a). A similar study with rotating bending fatigue tests was conducted by Xu et al. [44] on SLMed AlSi10Mg samples with four build directions. It was shown that the fatigue strength of 0° and 15° samples are higher than that of 45° and 90° sam-

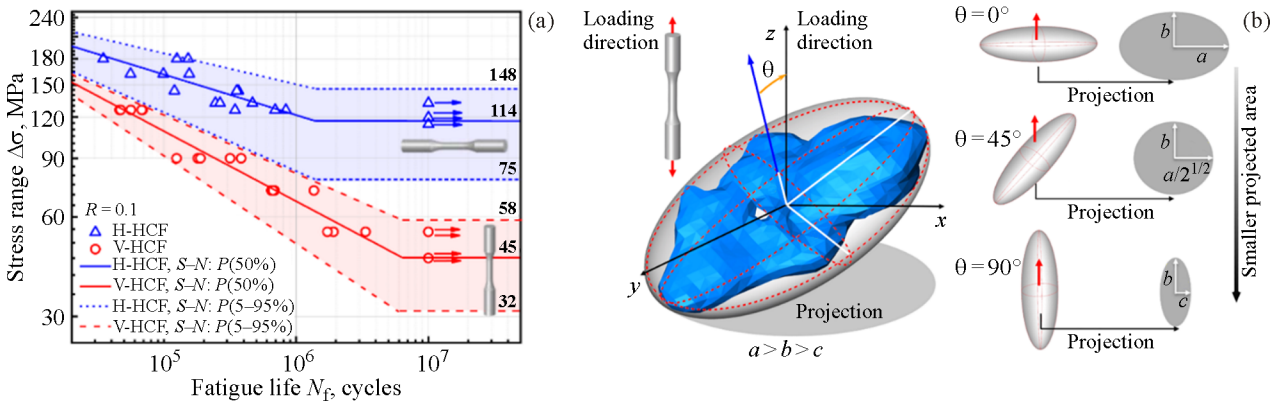

Fig. 7. Probabilistic *S–N* curves of horizontal (0°) and vertical SLMed AlSi10Mg samples (90°) in high cycle fatigue (a), spatial configuration of the defect with different orientation angles [52] (b) (color online).

ples. As for SLMed alloys, 0° samples usually show better fatigue strength than samples with other build directions. This is because the projected area of lack of fusion defects along the loading axis of 0° samples is smaller than that in samples with other directions (Fig. 7b).

In addition to the anisotropy of fatigue performance, defects have a pronounced volume effect due to the change in the so-called risk volume. The risk volume is defined as the volume with 90% of the maximum applied stress amplitude [69]. With the increase in sample volume, more large risk defects can be found. Therefore, samples with a larger volume show lower fatigue strength compared to samples with a small volume. For example, Tridello et al. [67] investigated the influence of geometrical size and build directions on the VHCF response of SLMed AlSi10Mg hourglass and Gaussian samples (Figs. 8a and 8b). It can be observed that the VHCF property of the Gaussian samples is much lower than that of the hourglass samples regardless of the building directions (Figs. 8c and 8d). Size-effects are more evident for SLMed samples than for conventionally built ones. This phenomenon must be carefully evaluated when considering the structural integrity of SLMed parts. For a more conservative evaluation of the fatigue property, it was suggested to use large-sized samples [69, 70].

3.2. Effect of Surface Treatment

SLMed structures typically show high surface roughness in the as-built condition due to the staircase effect and partially adhered molten powder par-

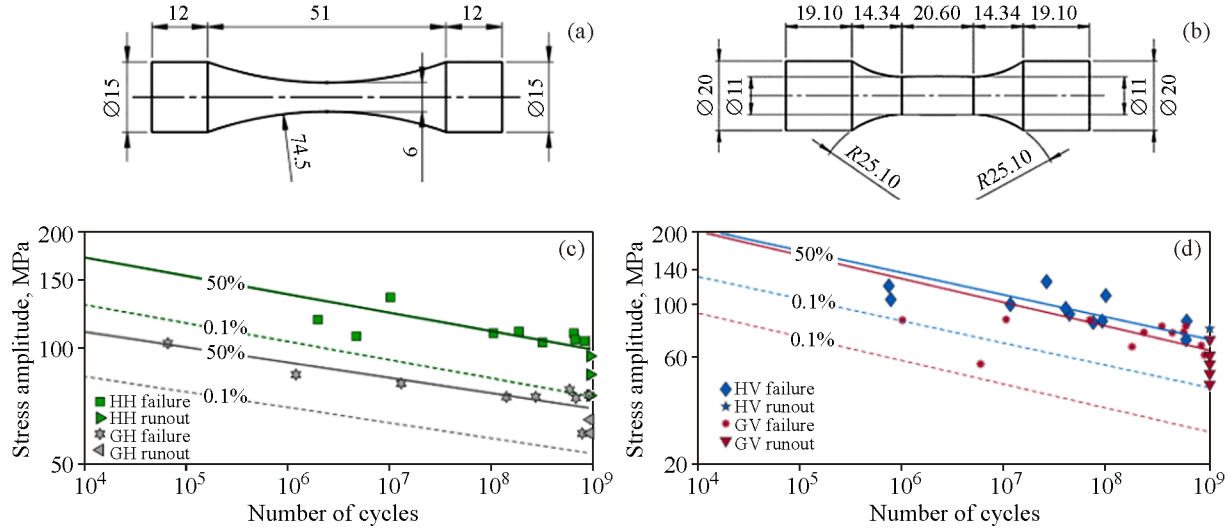

Fig. 8. Geometry of hourglass sample (a), geometry of Gaussian sample (b), median and 0.1% *P–S–N* curves of 90° samples (c), median and 0.1% *P–S–N* curves of 0° samples [67] (d) (color online).

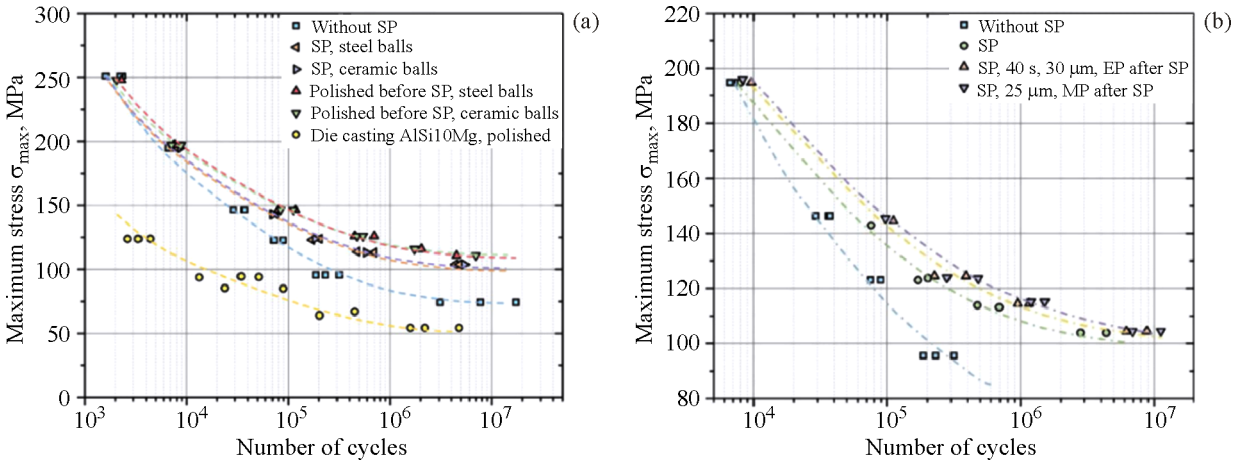

Fig. 9. *S–N* curves of SLMed and cast AlSi10Mg samples (a), *S–N* curves of shot-peened (SP) SLMed AlSi10Mg samples after mechanical (MP) or electrolytic polishing (EP) [25] (b) (color online).

ticles [63, 71, 72]. Similar to conventional alloys, surface defects lead to stress concentration and crack initiation when the structures are subjected to fatigue loading, resulting in a decrease of fatigue strength [18, 25, 30, 73–76]. In recent years, various surface treatment methods have been studied, such as electropolishing [25, 77], sandblasting [27, 78, 79], shot peening [25, 27, 80], and laser shock peening [81, 82]. Using these methods, the surface layer is subjected to plastic deformation accompanied by compressive residual stresses, grain refinement, and surface layer hardening, which is beneficial to the fatigue properties. Uzan et al. [25] studied the effect of shot peening on the fatigue behavior of SLMed AlSi10Mg. The results showed that shot peening can improve the fatigue performance of SLMed AlSi10Mg regardless of using steel balls or ceramic balls, and the fatigue strength of SLMed AlSi10Mg is higher than that of cast alloy (Fig. 9a). Further surface treatment of shot-peened samples with mechanical or electrolytic polishing only slightly improves the fatigue performance (Fig. 9b). Bagherifard et al. [27] studied the independent and combined effect of posttreatments, including shot peening, sandblasting, and heat treatment, on the fatigue behavior of SLMed AlSi10Mg. According to the results obtained, shot peening significantly improved the fatigue characteristics. However, the surface treatment led to a lower percentage of fatigue strength improvement in heat-treated samples compared to as-built samples.

3.3. Effect of Heterogeneous Microstructure

SLMed AlSi10Mg typically demonstrates heterogeneous melt pool characteristics. It was reported that the melt pool has different mechanical properties at the boundary and in the bulk. The latter shows higher hardness, yield stress, and flow stress [41]. This phenomenon is responsible for the appearance of an inhomogeneous plastic zone near the crack tip under cyclic loading. Xu et al. [44] studied the effect of build directions on the fatigue crack growth behavior of SLMed AlSi10Mg. Strain distributions obtained by finite element simulation and crack morphologies of 0°, 15°, 45°, and 90° samples are shown in Fig. 10. The results indicate that the crack growth path constantly interacts with the melt pool boundaries. The boundaries greatly affect crack propagation, and 90° samples show the worst crack growth behavior due to crack propagation along the melt pool boundaries. Awd et al. [66] reported that in 90° samples at a stress amplitude of 120 MPa the crack propagates along the melt pool boundaries, while at 100 MPa the crack path is different. This is because the elastic characteristics are more apparent when the external load is low. Therefore, the influence of melt pool boundaries on fatigue performance is more evident under high loads. In the VHCF region, Li et al. [83] observed secondary cracks on the longitudinal fracture surface using EBSD, as well as grain refinement at short cracks. The authors explained this by repeated cyclic pressing of the crack face. A nonuniform fine grain distribution is related to the crack propagation path, and the deflection of the growing crack promotes grain refinement (Fig. 11). Similar grain refinement phenomena have been reported for SLMed Ti6Al4V [84, 85]. A numerous cyclic pressing theory was proposed to explain this phenomenon [86].

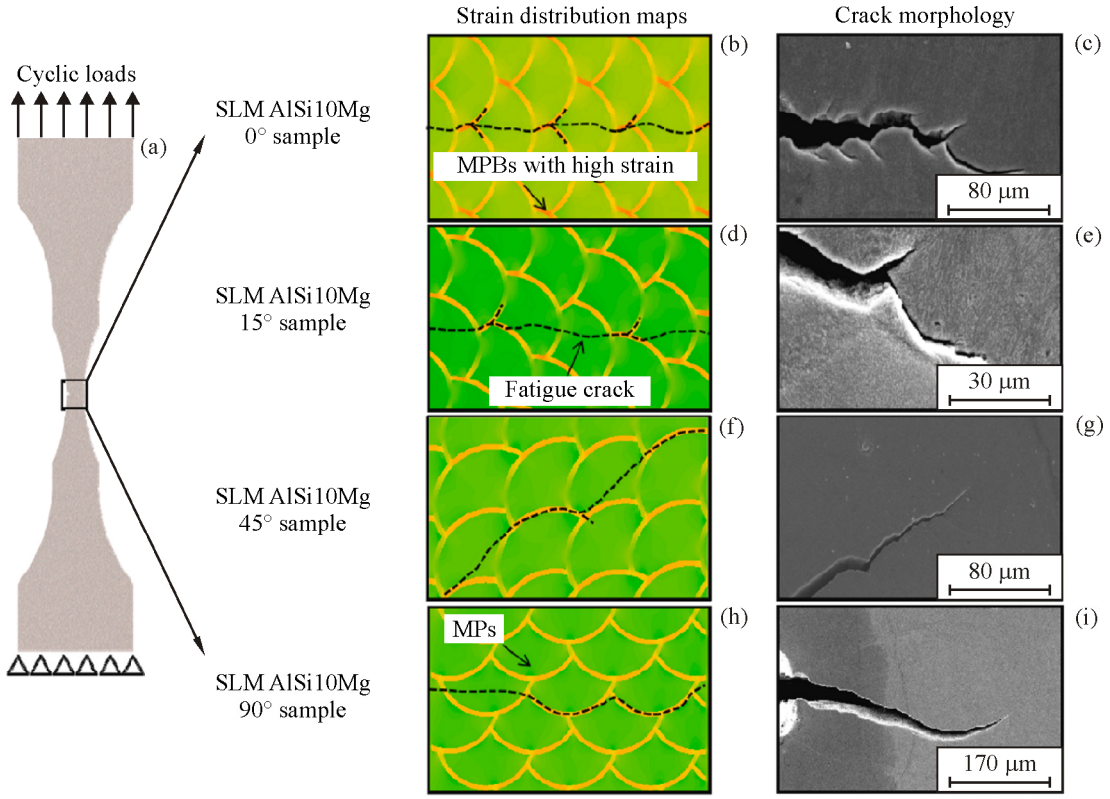

Fig. 10. Crack morphologies and strain distributions in 0°, 15°, 45°, and 90°SLMed AlSi10Mg samples [44] (color online).

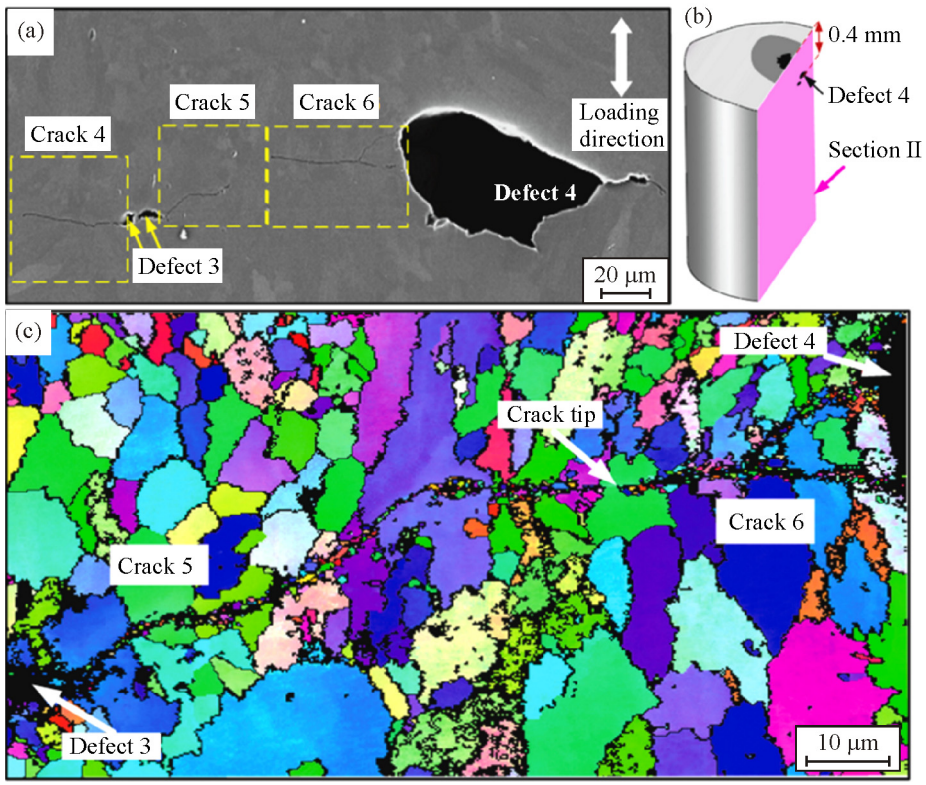

Fig. 11. SEM image of defect-induced cracking behavior in SLMed AlSi10Mg (a), location of the defect (b), EBSD IPF map of the crack growth path [83] (c) (color online).

3.4. Effect of Residual Stress

Fatigue and fracture failure modes in engineering applications are related to the stress state in the structure, so they are inevitably affected by the combination of loads and residual stresses in the components. When residual stresses are coupled with external loads, they threaten the structural integrity and cause a variety of failure modes [63, 87]. Residual stresses resulting from processing and posttreatment should be carefully assessed. However, it is not easy to separate the effect of residual stress on fatigue properties because the microstructure and porosity change during heat treatment. Recently, Tridello et al. [88] reported that the residual stress has a significant effect on the VHCF performance of SLMed AlSi10Mg. The VHCF response of samples annealed at 224°C for 2 h was higher than that of as-built samples. The influence of defects in samples annealed at 224°C for 2 h is more pronounced than in as-built samples, and the Vicker hardness of the two sample types is almost the same. Therefore, the difference in fatigue strength can be attributed to the process-induced residual stress. To reduce the residual stress effect in SLMed parts, heat treatment or powder bed preheating is usually recommended [89, 90]. It should be noted that heat treatment does not eliminate residual stresses, which affect the fatigue performance of parts during service. The effect of residual stress on the fatigue performance of SLMed AlSi10Mg has not yet been well understood and more mechanisms need to be clarified in the future.

3.5. Effect of Heat Treatment and Hot Isostatic Pressing

Owing to the heterogeneous microstructures and significant residual stresses in SLMed structures, heat treatment is frequently recommended to homogenize the microstructure and release the residual stresses. There are a lot of studies examining the effect of different heat treatment schedules, mainly T6 heat treatment and annealing at different temperatures [29–32]. T6 heat treatment is commonly used in conventional Al-Si alloys because they can achieve maximum precipitation hardening during this heat

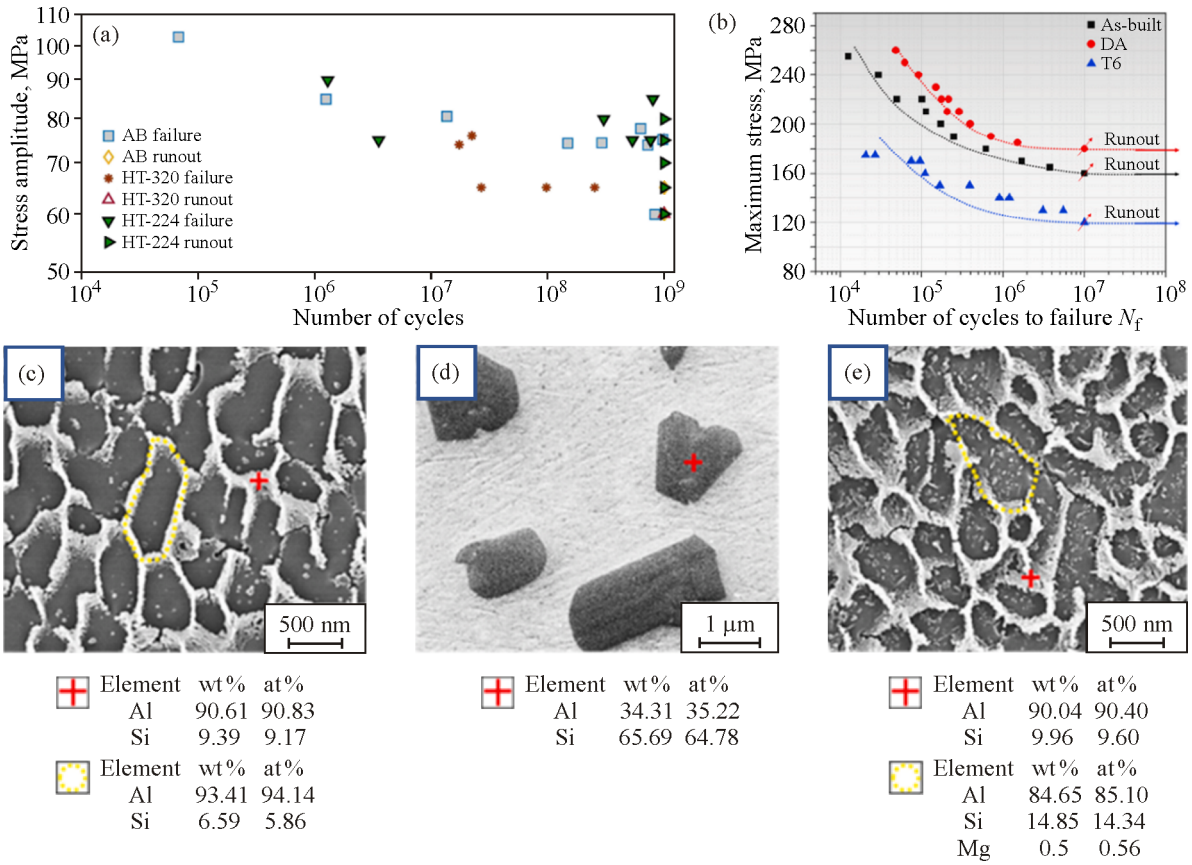

Fig. 12. *S–N* curves of as-built samples and annealed for 2 h at 320°C and for 2 h at 224°C [25] (a), *S–N* curves of as-built, directly aged, and T6 samples [31] (b), typical microstructure of as-built, T6, and directly aged samples [31] (c–e) (color online).

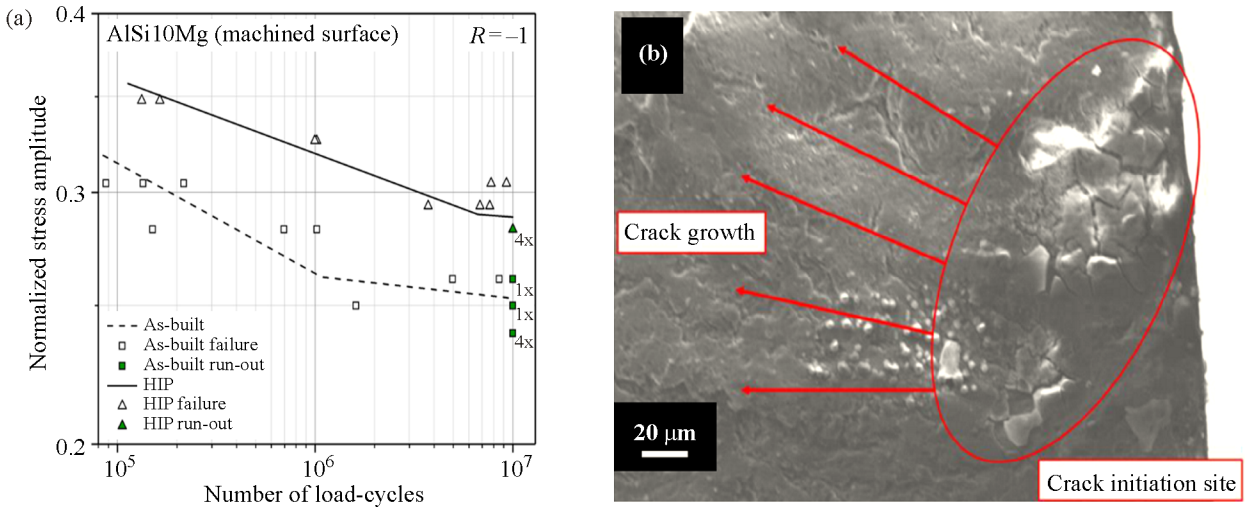

Fig. 13. *S–N* curves of as-built samples and subjected to hot isostatic pressing (HIP) (a), fracture surface of a HIPed sample [37] (b) (color online).

treatment schedule. Interestingly, several studies reported that the tensile and fatigue strength decreases significantly after T6 heat treatment [31, 32]. This is because T6 heat treatment significantly changes the microstructure. The coarsening of the Si network decreases the fatigue strength of SLMed AlSi10Mg. That is why conventional T6 heat treatment is not suitable for SLMed AlSi10Mg, for which a unique heat treatment process should be established. Tridello et al. [29] studied the effect of annealing on the VHCF response of SLMed AlSi10Mg with two different annealing schedules: annealing at 320°C for 2 h and at 224°C for 2 h. After 2 h annealing at 320°C, the Si phase was spheroidized, and the fatigue performance of SLMed AlSi10Mg deteriorated. On the contrary, 2 h annealing at 224°C slightly improved the fatigue properties (Fig. 12a). Recently, Baek et al. [31] studied the effect of direct aging on the fatigue behavior of SLMed AlSi10Mg and compared the results with as-built and T6 samples. As shown in Fig. 12b, the aged samples show outstanding fatigue strength compared with the as-built and T6 samples. Direct aging may be a promising heat treatment method for SLMed AlSi10Mg. Figures 12c–12e illustrate the typical microstructure of as-built, T6, and directly aged samples. The fatigue strength improvement of aged samples can be attributed to their cellular structural morphology characterized by a large amount of fine Si precipitates (Fig. 12e). It should be noted that heat treatment does not close defects in SLMed Al-Si alloys. Hence, the improvement of fatigue performance by heat treatment is always limited.

Hot isostatic pressing (HIP) has proved to be a powerful method of reducing defects in some SLMed alloys, such as Ti6Al4V [33, 35] and Inconel 718 [91, 92]. However, the studies dealing with the effect of HIP on SLMed AlSi10Mg are still rare [36, 37, 93]. For cast Al-Si alloy, HIP is a direct method of reducing porosity. Only a slight change in microstructural characteristics leads to a significant increase in fatigue strength. When applied to SLMed AlSi10Mg, HIP at elevated temperatures causes breaking of the Si network into individual particles. Hence the fatigue strength decreases significantly, although defects are reduced considerably [75]. A recent study by Schneller et al. [37] revealed that HIP treatment above the solubility temperature with subsequent low-temperature annealing has a beneficial effect on the fatigue strength of SLMed AlSi10Mg (Fig. 13a). The crack initiation mode also changes after HIP: fatigue cracks no longer initiate at lack of fusion defects but at microstructural defects produced by pressing (Fig. 13b) [37].

3.6. Fracture Behavior

Fracture mechanics is often used to evaluate structures with preexisting cracks. Fracture toughness is an essential parameter when assessing the quality of typical engineering structures, especially pipelines, automobiles, ships, and aircraft. Paul et al. [45] reported that the fracture toughness of SLMed AlSi10Mg with different process parameters is 19–30 MPa $m^{1/2}$, which is higher than the average

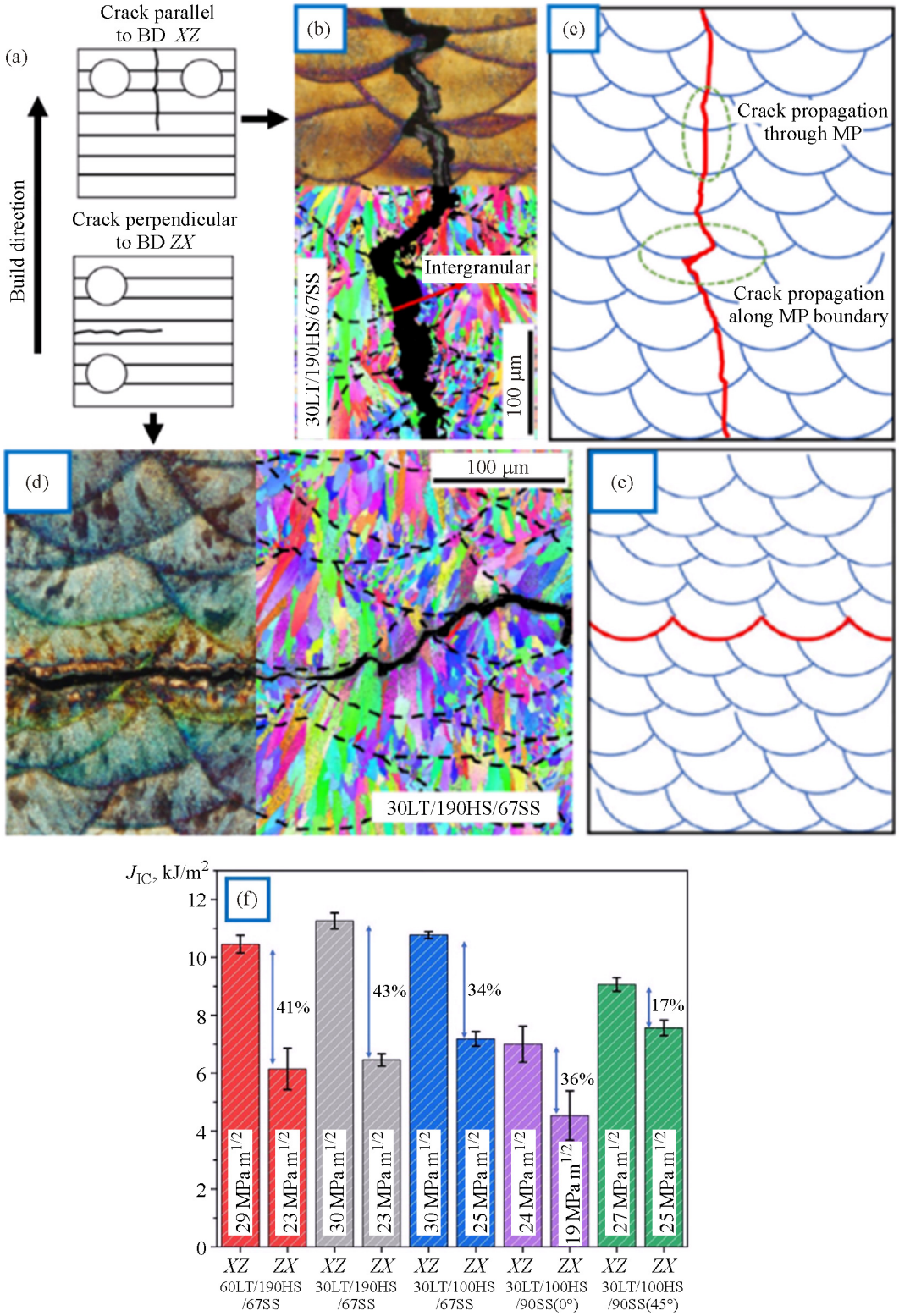

Fig. 14. Crack orientation of samples (a), crack propagation path in *XZ* samples (b), schematic representation of crack path in *XZ* samples (c), crack propagation path analysis in *ZX* samples (d), schematic representation of crack path in *ZX* samples (e), J_{Ic} values of all build conditions [45] (f) (color online).

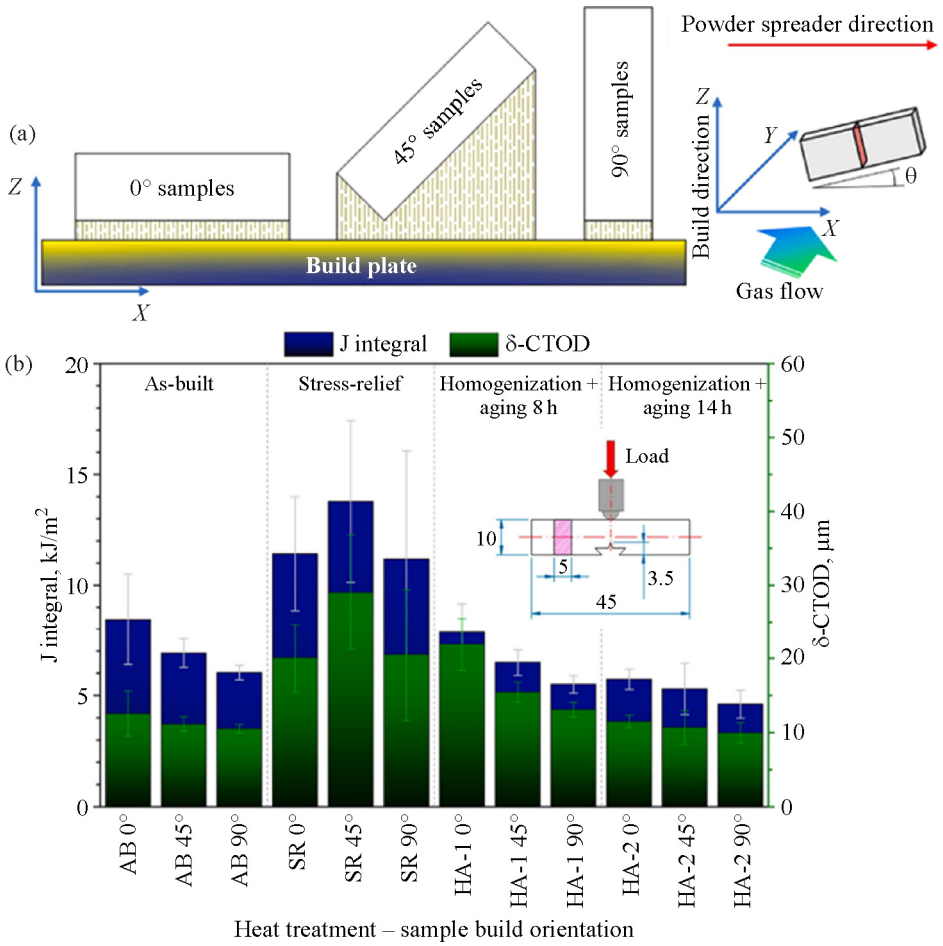

Fig. 15. Build directions of samples (a), fracture toughness δ-CTOD and J-integral of SLMed AlSi10Mg with different heat treatment conditions and build directions [94] (b) (color online).

fracture toughness of cast AlSi10Mg equal to 18.6 MPa $m^{1/2}$. The results indicate that the process parameters greatly influence fracture toughness, and the effect of the scanning strategy is more pronounced than that of the layer thickness and hatch spacing. In addition, the crack propagation is strongly affected by the melt pool characteristics due to the relatively weak mechanical properties of the melt pool boundary. Figure 14a shows the crack propagation paths in samples built in two different directions. In the *XZ* samples, the crack propagates mainly within the melt pool and has a tortuous path caused by deflection at the pool boundary (Figs. 14b, 14c). In the *ZX* samples, the crack travels mostly along the melt pool boundary (Figs. 14d, 14e). This behavior leads to a significant anisotropy of fracture toughness of SLMed AlSi10Mg (Fig. 14f). Araújo et al. [94] studied the effect of build direction and different heat treatment schedules on the tensile and fracture properties of SLMed AlSi10Mg. It was found that the samples subjected to stress relief annealing at 300°C for two hours have the highest fracture toughness. The 90° samples have the lowest average fracture toughness values depending on the heat treatment conditions (Fig. 15).

Defects and heterogeneous microstructure greatly affect the fracture toughness. Recently, attempts have been made to investigate these effects by numerical modeling. Muro-Barrios et al. [95] studied the impact of dual-scale porosity on crack growth in additively manufactured alloys based on the Gurson–Tvergaard–Needleman model. Simulations allowed visualizing the void growth, interaction and coalescence mechanisms in additively manufactured Ti6Al4V. It was found that random defects can temporarily increase or decrease local toughness, depending on their position relative to the crack tip. This means that defects can be intentionally introduced in SLMed alloys during the SLM process in order to increase the fracture properties. Regarding the effect of heteroge-

neous microstructure, Jamshidian et al. [96] studied the influence of melt pool characteristics on the fracture behavior of SLMed Al-12Si alloy based on a cohesive model. It was shown that the melt pool geometry has a considerable effect on the fracture toughness and results in significant anisotropy. The pool geometry can be better altered via simulations to obtain higher fracture toughness.

3.7. Fatigue Modeling Methods

Prediction of the fatigue strength and fatigue life of SLMed parts is of great importance for critical structure assessment. Several models have been developed to predict the fatigue performance of SLMed AlSi10Mg.

Since defects in SLMed alloys can be considered as short cracks, the method based on fracture mechanics appears to be promising. The parameter of the square root of the defect area $\sqrt{\text{area}}$ proposed by Murakami et al. [97] has been widely used to characterize the size of defects in SLMed alloys. It is generally considered that the fatigue life is controlled by the maximum defect in the control volume. Extreme value statistics methods are usually used to estimate the maximum defect of parts with different volumes [98, 99]. After the maximum defect size is determined, empirical formulas or fracture mechanics models can be used to estimate the fatigue strength and fatigue life under different loading conditions.

As shown in Eq. (1), concerning the fatigue limit prediction, the semi-empirical formula proposed for steels by Murakami seems to have a great potential for SLMed alloys [48, 99, 100]:

$$\sigma_w = \frac{C(\text{HV}+120)}{(\sqrt{\text{area}})^{1/6}}, \tag{1}$$

where σ_w is the fatigue limit, HV is the Vickers hardness, and C is the constant. There are three types of defects, including surface, subsurface, and internal defects, with C equal to 1.43, 1.41, and 1.56, respectively. However, applying this method to nonferrous metals such as Al-alloys seems unpractical. For al-alloys, the term 120 should be adjusted based on the elastic moduli of two materials:

$$\sigma_w = \frac{C(\text{HV}+120E_{Al}/E_{st})}{(\sqrt{\text{area}})^{1/6}}, \tag{2}$$

where E_{Al} is the elastic modulus of Al-alloys, and E_{st} is the elastic modulus of stainless steel. The applicability of this method for the prediction of fatigue strength of SLMed AlSi10Mg has been proved by Xu et al. [48]. It should be noted that Eqs. (1) and (2) cannot be used to calculate the fatigue life. Therefore, Wang et al. [101] proposed a modified equation:

$$\sigma_w = (\alpha - \beta \log N_f)\frac{\text{HV}+120}{(\sqrt{\text{area}})^{1/6}}, \tag{3}$$

where N_f is the fatigue life, α and β are the fitting constants based on the *S–N* data. Zhang et al. [102] used this method to predict the fatigue life of SLMed AlSi10Mg samples with different build directions. The predicted results were in good agreement with the experimental data.

The Kitagawa–Takahashi (K–T) diagram [103] describes the variation of fatigue limit with defect size in a semi-empirical way. Unless the defect is larger than a safe defect size, it will not propagate. The fatigue limit decreases with increasing defect size when the defect size exceeds the safe defect size [50, 52]. Moreover, the K–T diagram can determine a safe life region, which can be used to evaluate the life of engineering structures with cracks. In order to consider the effect of small cracks, the K–T diagram should be modified using the El-Haddad model, as described in Eqs. (4) and (5) [52, 104]:

$$\Delta\sigma_w = \Delta\sigma_{w0}\sqrt{\frac{\sqrt{\text{area}}}{\sqrt{\text{area}}+\sqrt{\text{area}_0}}}, \tag{4}$$

$$\Delta K_{th} = \Delta K_{th,lc}\sqrt{\frac{\sqrt{\text{area}}}{\sqrt{\text{area}}+\sqrt{\text{area}_0}}}, \tag{5}$$

$$\sqrt{\text{area}_0} = \frac{1}{\pi}\left(\frac{\Delta K_{th,lc}}{Y\Delta\sigma_{w0}}\right)^2, \tag{6}$$

where $\Delta\sigma_w$ is the fatigue limit of the material with defects, $\Delta\sigma_{w0}$ is the fatigue limit without defects, and $K_{th,1c}$ is the threshold value of long crack propagation in the material. The quantity $\sqrt{\text{area}_0}$ can be calculated according to Eq. (6), where Y is 0.5 for internal defects and Y is 0.65 for surface defects.

Beretta et al. [105] summarized the fatigue data on additively manufactured AlSi10Mg and Ti6Al4V and established the K–T diagram using the parameter in terms of the EI-Haddad model. Wu et al. [52] plotted the K–T diagram based on the defect size distribution from computed tomography data. The fatigue limit distribution of the samples with two different build directions was determined as shown in Fig. 16a. Considering the residual stress, Beretta et al. [63] studied the effect of build direction on the fatigue properties of as-built SLMed AlSi10Mg samples. The residual stress was regarded as a stress ratio in the K–T diagram (Fig. 16b). It can be used to evaluate

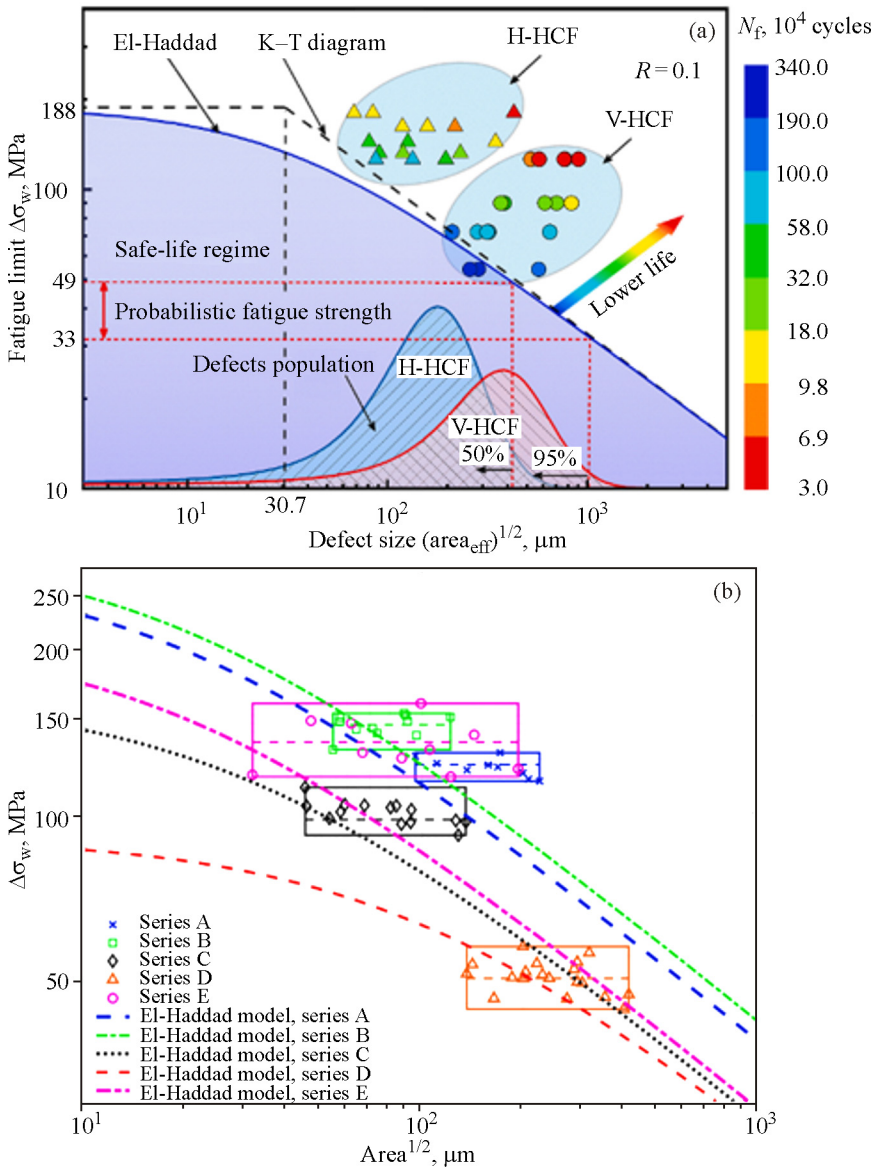

Fig. 16. Probabilistic Kitagawa–Takahashi diagram described by the El-Haddad formulation considering the defect distribution [52] (a), Kitagawa–Takahashi diagram described by the El-Haddad formulation of SLMed AlSi10Mg considering the residual stress [63] (b) (color online).

the fatigue limit of SLMed parts in the as-built condition. Hu et al. [99] proposed a modified K–T diagram based on the NASGRO equation for residual life prediction of alloys.

The fatigue crack growth model has also been widely used to predict the fatigue life of SLMed alloys. Romano et al. [50] conducted fatigue tests on three batches of SLMed AlSi10Mg samples (Fig. 17) and established the relationship between the defect size and fatigue life using the NASGRO code, according to the equation

$$\frac{da}{dN} = C\left(\frac{1-f}{1-R}\Delta K\right)^n \frac{(1-\Delta K_{th}/\Delta K)^p}{(1-K_{max}/K_c)^q}, \qquad (7)$$

where da/dN is the fatigue crack growth rate, f is the crack opening function, R is the stress ratio, C, n, p, and q are the fitting parameters, K_{max} and K_c are the maximum and critical stress intensity factors. The prediction results obtained on the basis of linear elastic fracture mechanics agreed with the experimental fatigue data for the high-cycle fatigue conditions. However, plastic correction was required for the low-cycle fatigue regime.

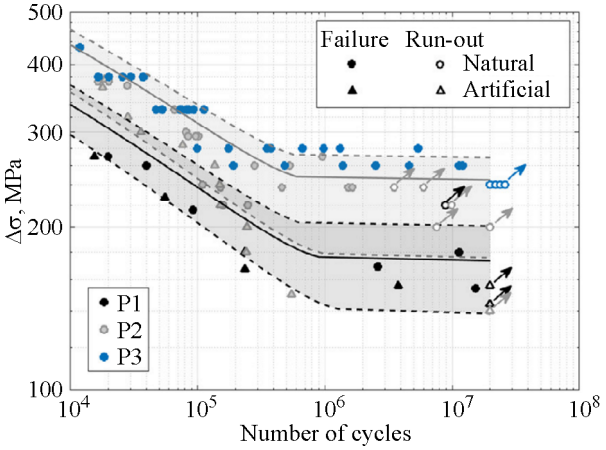

Fig. 17. Fatigue life prediction for three batches of SLMed AlSi10Mg samples based on the NASGRO code [50] (color online).

Similar studies were carried out on other SLMed alloys. Greitemeier et al. [106] studied the effect of surface roughness on the fatigue behavior of SLMed Ti6Al4V. The authors used the equivalent initial flaw size approach to find the relationship between the equivalent flaw size and fatigue life. Yadollahi et al. [107] investigated the effects of surface roughness, defect size, and shape on the fatigue strength of additively manufactured Ni-718 alloys using the fracture mechanics method. The maximum valley depth of the surface profile was used as the initial defect size to predict the fatigue life of SLMed alloys with the as-built surface. Then, Yadollahi et al. [108] studied the effect of heat treatment and build direction on the fatigue performance of 17-4 precipitation hardening stainless steel and established the relationship between defect size and fatigue life by FASTRAN using the equivalent and real initial flaw sizes. The fatigue life was overestimated when using the real initial flaw size. It should be noted that the void interaction and crack coalescence should not be ignored when many large voids are present.

Crack initiation consumes most of the fatigue life for SLMed AlSi10Mg in the HCF and VHCF region. Irreversible dislocation slip in plastic zones near defects significantly affects crack initiation. The dislocation dipole accumulation theory proposed by Tanaka and Mura [109] can be used to predict the crack initiation life. Based on this model, Zhang et al. [102] proposed a fatigue life prediction model considering the stress concentration effect of the defect, and there was good agreement between experimental and predicted data. Nadot et al. [110] developed a framework for predicting the fatigue life based on the defect stress gradient models taking into account the defect type, size, position, morphology, and loading effect. As shown in Fig. 18, the prediction process is as follows: (i) obtaining an X-ray microcomputed

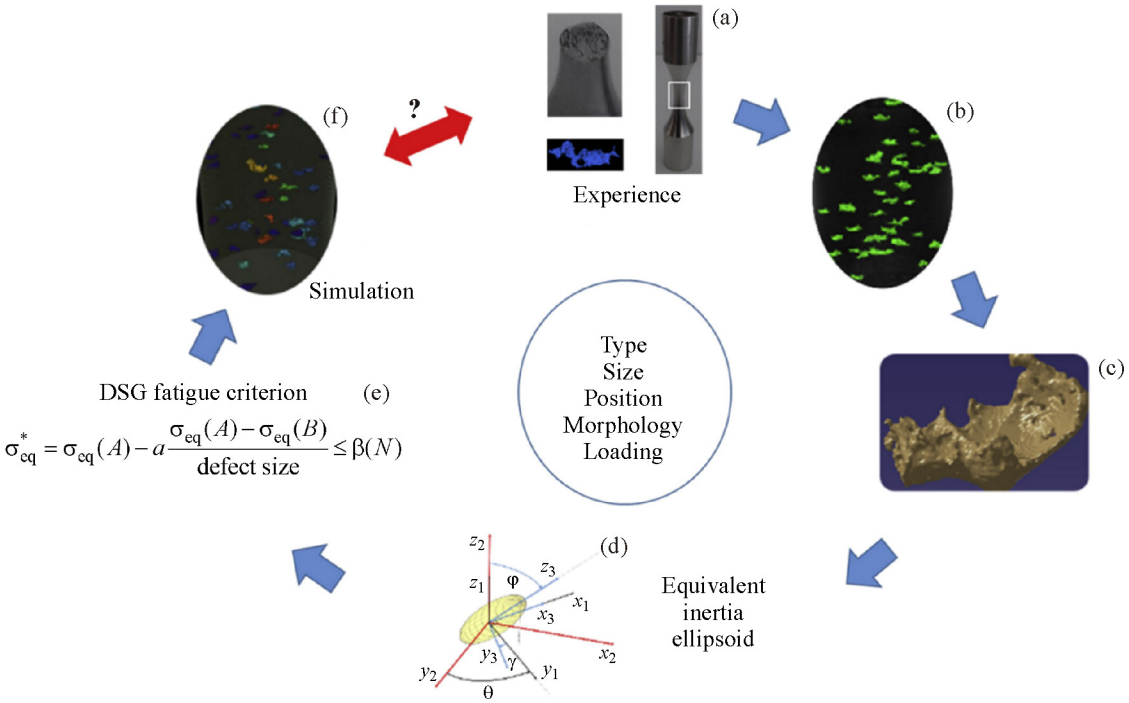

Fig. 18. The modeling strategy to evaluate the influence of defect morphology on fatigue limit [110] (color online).

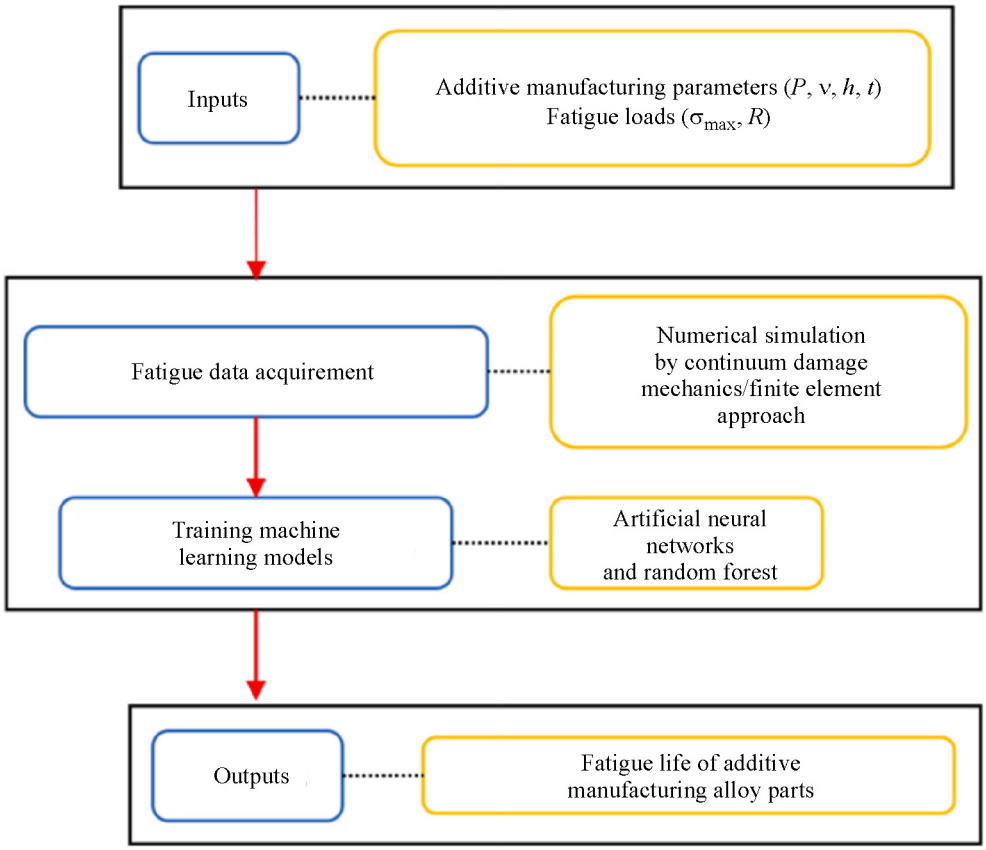

Fig. 19. A flowchart illustrating the machine learning strategy for fatigue life prediction of additively manufactured alloys [117].

tomography 3D image of the material, (ii) computing the equivalent inertia ellipsoid of each individual pore, (iii) modeling the influence of the defect on the fatigue limit using the defect stress gradient approach coupled with the Eshelby theory, and (iv) 3D mapping the criticality of each defect.

The models based on the crystal plasticity finite element method (CPFEM) can be used to capture the inhomogeneous mechanical response at the grain scale. Zhang et al. [111] developed a model using CPFEM and Voronoi tessellation to study the HCF and VHCF properties of SLMed AlSi10Mg. It was found that the accumulation of cyclic plastic strain near a pore is significantly higher than that near an inclusion. This residual stress caused pronounced plastic strain localization near an inclusion, adversely affecting the fatigue performance. The Morrow and Smith–Watson–Topper models were used to predict the fatigue life. The results showed that the Smith–Watson–Topper model agreed well with the experimental life observed between 10^5–10^9. Zhang et al. [112] allied CPFEM to study crack initiation behaviors in SLMed AlSi10Mg. The results showed that plastic strain accumulates at defects, while residual stress accumulates at an inclusion during cyclic loading. It is generally recognized that plastic strains and local stresses are critical for crack initiation. A new fatigue prediction model was proposed for fatigue life prediction of SLMed AlSi10Mg. The fatigue indicator parameter (FIP) was taken as the increment of the accumulation of plastic strain P_{ac} in stable loading cycles. The value of P_{ac} can be estimated by the integral of the double dot product of the plastic velocity gradient $\mathbf{L}_p$:

$$P_{ac} = \int \sqrt{\frac{2}{3}} \mathbf{L}_p : \mathbf{L}_p \mathrm{d}t, \tag{8}$$

$$\mathrm{FIP} = \Delta P_{ac} = P_{ac}\big|_{N+1} - P_{ac}\big|_{N}. \tag{9}$$

The fatigue life can be predicted by the following formula:

$$N_p = \frac{\alpha_p}{d_{gr}(\mathrm{FIP})^2}, \tag{10}$$

where d_{gr} is a reference constant, which is on the order of the grain size to represent the microstructure, and α_p is a fitting constant.

As mentioned earlier, the fatigue properties of SLMed alloys are affected by many process parameters and posttreatment methods. In recent years, the machine learning approach has shown great potential for fatigue life measurements as an efficient tool for studying the relationship between multiple factors [113–116]. One of the main problems in the application of machine learning to fatigue life prediction is that the data sets obtained from experiments are usually small. The most common methods for expanding the fatigue data sets are based on finite element simulation [113, 117] or Monte Carlo simulation [114]. Zhan et al. [113, 117] developed a data-driven machine learning framework for the fatigue life prediction of SLMed alloys using a continuum damage mechanics theory to expand the fatigue data set (Fig. 19). The effect of different process parameters and fatigue loads on the fatigue performance can be captured within this framework. Maleki et al. [115] used artificial neural networks to evaluate the fatigue behavior of posttreated V-notched SLMed AlSi10Mg samples. The authors studied the individual and combined effects of various posttreatments on microstructure, surface state, microhardness, porosity, residual stress, and fatigue behavior.

4. CONCLUSIONS

This review summarized the current state of the art for the fatigue and fracture studies of SLMed AlSi10Mg. The conclusions and prospects that can be drawn are as follows.

Fatigue and fracture properties of SLMed AlSi10Mg are influenced by the combination of defect characteristics, microstructural features, and residual stresses. When SLMed structures are subjected to fatigue loading, cracks tend to initiate from lack of fusion defects.

The conventional T6 heat treatment procedure is not suitable for SLMed Al-Si alloys. High-temperature heat treatment and hot isostatic pressing break up the Si network structure and reduce the mechanical properties of SLMed AlSi10Mg. Direct aging and low-temperature annealing seem suitable for SLMed AlSi10Mg alloys. Heat treatment processes for the postprocessing of SLMed parts still need further investigation. The residual stress caused by the SLM process has a negative effect on the fatigue performance. Preheating the substrate or annealing can reduce the residual stress effect.

Due to different mechanical properties between the boundary and the bulk of the melt pool, the melt pool boundary provides a weak interface for crack propagation. During the fatigue crack growth, the plastic strain is more likely to accumulate at the melt pool boundary, significantly affecting the fatigue crack growth behavior.

SLMed AlSi10Mg often demonstrates unique toughening mechanisms. The defects and melt pool characteristics near the crack tip can increase or decrease the fracture toughness of SLMed alloys. Since SLM offers a unique opportunity for the design of materials, more toughening mechanisms based on the design freedom should be provided in the future.

SLM is a near-net forming technology, and any postprocessing reduces its molding advantages. In addition, postprocessing significantly increases the time and cost of the additive process. Heat treatment and hot isostatic pressing affect the dimensional accuracy of SLMed parts. Therefore, further parameter optimization is needed to provide the opportunity of using SLMed alloys directly in engineering applications without posttreatment.

FUNDING

This work was funded by the National Natural Science Foundation of China (Nos. 11932020, 12072345), and National Science and Technology Major Project (J2019-VI-0012-0126) and Science Center for Gas Turbine Project (P2022-B-III-008-001).

REFERENCES

1. Herzog, D., Seyda, V., Wycisk, E., and Emmelmann, C., Additive Manufacturing of Metals, A*cta Mater*., 2016, vol., 117, pp. 371–392. https://doi.org/10.1016/j.actamat.2016.07.019
2. Gu, D., Shi, X., Poprawe, R., Bourell, D.L., Setchi, R., and Zhu, J., Material–Structure–Performance Integrated Laser-Metal Additive Manufacturing, *Science*, 2021, vol. 372. https://doi.org/10.1126/science.abg1487
3. Prathyusha, A.L.R. and Raghu Babu, G., A Review on Additive Manufacturing and Topology Optimization Process for Weight Reduction Studies in Various Industrial Applications, *Mater. Today Proc*., 2022, vol. 62, pp. 109–117. https://doi.org/10.1016/j.matpr.2022.02.604
4. Matsko, A. and França, R., Design, Manufacturing and Clinical Outcomes for Additively Manufactured Titanium Dental Implants: A Systematic Review, *Dent. Rev*., 2022, vol. 2, p. 100041. https://doi.org/10.1016/j.dentre.2022.100041
5. Kumar, R., Kumar, M., and Chohan, J.S., The Role of Additive Manufacturing for Biomedical Applications:

A Critical Review, *J. Manuf. Process.*, 2021, vol. 64, pp. 828–850. https://doi.org/10.1016/j.jmapro.2021.02.022

6. Kareem, F.A. and Michael, P.A., An Investigation on Applications of Additive Manufacturing of Electrical Machines, *Mater. Today Proc*., 2022, vol. 58, pp. 86–90. https://doi.org/10.1016/j.matpr.2021.12.590
7. Olakanmi, E.O., Cochrane, R.F., and Dalgarno, K.W., A Review on Selective Laser Sintering/Melting (SLS/SLM) of Aluminium Alloy Powders: Processing, Microstructure, and Properties, *Progr. Mater. Sci*., 2015, vol. 74, pp. 401–477. https://doi.org/10.1016/j.pmatsci.2015.03.002
8. Aboulkhair, N.T., Simonelli, M., Parry, L., Ashcroft, I., Tuck, C., and Hague, R., 3D Printing of Aluminium Alloys: Additive Manufacturing of Aluminium Alloys Using Selective Laser Melting, *Progr. Mater. Sci*., 2019, vol. 106, p. 100578. https://doi.org/10.1016/j.pmatsci.2019.100578
9. Ding, Y., Muñiz-Lerma, J.A., Trask, M., Chou, S., Walker, A., and Brochu, M., Microstructure and Mechanical Property Considerations in Additive Manufacturing of Aluminum Alloys, *MRS Bull*., 2016, vol. 41, pp. 745–751. https://doi.org/10.1557/mrs.2016.214
10. Martin, J.H., Yahata, B.D., Hundley, J.M., Mayer, J.A., Schaedler, T.A., and Pollock, T.M., 3D Printing of High-Strength Aluminium Alloys, *Nature*, 2017, vol. 549, pp. 365–369. https://doi.org/10.1038/nature23894
11. Bi, J., Lei, Z., Chen, Y., Chen, X., Tian, Z., Liang, J., Zhang, X., and Qin, X., Microstructure and Mechanical Properties of a Novel Sc and Zr Modified 7075 Aluminum Alloy Prepared by Selective Laser Melting, *Mater. Sci. Eng. A*, 2019, vol. 768, p. 138478. https://doi.org/10.1016/j.msea.2019.138478
12. Bayoumy, D., Boll, T., Schliephake, D., Wu, X., Zhu, Y., and Huang, A., On the Complex Intermetallics in An Al-Mn-Sc Based Alloy Produced by Laser Powder Bed Fusion, *J. Alloys Compd*., 2022, vol. 901, p. 163571. https://doi.org/10.1016/j.jallcom.2021.163571
13. Jia, Q., Zhang, F., Rometsch, P., Li, J., Mata, J., Weyland, M., Bourgeois, L., Sui, M., and Wu, X., Precipitation Kinetics, Microstructure Evolution and Mechanical Behavior of a Developed Al–Mn–Sc Alloy Fabricated by Selective Laser Melting, *Acta Mater.*, 2022, vol. 193, pp. 239–251. https://doi.org/10.1016/j.actamat.2020.04.015
14. Feng, Z., Tan, H., Fang, Y., Lin, X., and Huang, W., Selective Laser Melting of TiB_2/AlSi10Mg Composite: Processability, Microstructure and Fracture Behavior, *J. Mater. Process. Technol.*, 2022, vol. 299, p. 117386. https://doi.org/10.1016/j.jmatprotec.2021.117386
15. Li, X.P., Ji, G., Chen, Z., Addad, A., Wu, Y., Wang, H.W., Vleugels, J., Van Humbeeck, J., and Kruth, J.P., Selective Laser Melting of Nano-TiB_2 Decorated AlSi10Mg Alloy with High Fracture Strength and Ductility, *Acta Mater*., 2017, vol. 129, pp. 183–193. https://doi.org/10.1016/j.actamat.2017.02.062
16. Sanaei, N. and Fatemi, A., Defects in Additive Manufactured Metals and Their Effect on Fatigue Performance: A State-of-the-Art Review, *Progr. Mater. Sci*., 2021, vol. 117, p. 100724. https://doi.org/10.1016/j.pmatsci.2020.100724
17. Becker, T.H., Kumar, P., and Ramamurty, U., Fracture and Fatigue in Additively Manufactured Metals, *Acta Mater*., 2021, vol. 219, p. 117240. https://doi.org/10.1016/j.actamat.2021.117240
18. Fatemi, A., Molaei, R., Simsiriwong, J., Sanaei, N., Pegues, J., Torries, B., Phan, N., and Shamsaei, N., Fatigue Behaviour of Additive Manufactured Materials: An Overview of Some Recent Experimental Studies on Ti-6Al-4V Considering Various Processing and Loading Direction Effects, *Fatigue Fract. Eng. Mater. Struct*., 2019, vol. 42, pp. 991–1009. https://doi.org/10.1111/ffe.13000
19. Qian, G., Li, Y., Paolino, D.S., Tridello, A., Berto, F., and Hong, Y., Very-High-Cycle Fatigue Behavior of Ti-6Al-4V Manufactured by Selective Laser Melting: Effect of Build Orientation, *Int. J. Fatigue*, 2020, vol. 136, p. 105628. https://doi.org/10.1016/j.ijfatigue.2020.105628
20. Qian, G., Jian, Z., Qian, Y., Pan, X., Ma, X., and Hong, Y., Very-High-Cycle Fatigue Behavior of AlSi10Mg Manufactured by Selective Laser Melting: Effect of Build Orientation and Mean Stress, *Int. J. Fatigue*, 2020, vol. 138, p. 105696. https://doi.org/10.1016/j.ijfatigue.2020.105696
21. Thijs, L., Kempen, K., Kruth, J.P., and Van Humbeeck, J., Fine-Structured Aluminium Products with Controllable Texture by Selective Laser Melting of Pre-Alloyed AlSi10Mg Powder, *Acta Mater*., 2013, vol. 61, pp. 1809–1819. https://doi.org/10.1016/j.actamat.2012.11.052
22. Delahaye, J., Tchuindjang, J.T., Lecomte-Beckers, J., Rigo, O., Habraken, A.M., and Mertens, A., Influence of Si Precipitates on Fracture Mechanisms of AlSi10Mg Parts Processed by Selective Laser Melting, *Acta Mater.*, 2019, vol. 175, pp. 160–170. https://doi.org/10.1016/j.actamat.2019.06.013
23. Fang, Z.C., Wu, Z.L., Huang, C.G., and Wu, C.W., Review on Residual Stress in Selective Laser Melting Additive Manufacturing of Alloy Parts, *Opt. Laser Technol*., 2020, vol. 129, p. 106283. https://doi.org/10.1016/j.optlastec.2020.106283
24. Yadollahi, A. and Shamsaei, N., Additive Manufacturing of Fatigue Resistant Materials: Challenges and Opportunities, *Int. J. Fatigue*, 2017, vol. 98, pp. 14–31. https://doi.org/10.1016/j.ijfatigue.2017.01.001
25. Uzan, N.E., Ramati, S., Shneck, R., Frage, N., and Yeheskel, O., On the Effect of Shot-Peening on Fatigue Resistance of AlSi10Mg Specimens Fabricated

by Additive Manufacturing Using Selective Laser Melting (AM-SLM), *Addit. Manuf.*, 2018, vol. 21, pp. 458–464. https://doi.org/10.1016/j.addma.2018.03.030
26. Yu, W., Sing, S.L., Chua, C.K., and Tian, X., Influence of Re-Melting on Surface Roughness and Porosity of AlSi10Mg Parts Fabricated by Selective Laser Melting, *J. Alloys Compd*., 2019, vol. 792, pp. 574–581. https://doi.org/10.1016/j.jallcom.2019.04.017
27. Bagherifard, S., Beretta, N., Monti, S., Riccio, M., Bandini, M., and Guagliano, M., On the Fatigue Strength Enhancement of Additive Manufactured Al Si10Mg Parts by Mechanical and Thermal Post-Processing, *Mater. Des*., 2018, vol. 145, pp. 28–41. https://doi.org/10.1016/j.matdes.2018.02.055
28. Romano, S., Nezhadfar, P.D., Shamsaei, N., Seifi, M., and Beretta, S., High Cycle Fatigue Behavior and Life Prediction for Additively Manufactured 17-4 PH Stainless Steel: Effect of Sub-Surface Porosity and Surface Roughness, *Theor. Appl. Fract. Mech*., 2020, vol. 106. https://doi.org/10.1016/j.tafmec.2020.102477
29. Tridello, A., Fiocchi, J., Biffi, C.A., Chiandussi, G., Rossetto, M., Tuissi, A., and Paolino, D.S., Influence of the Annealing and Defects on the VHCF Behavior of an SLM AlSi10Mg Alloy, *Fatigue Fract. Eng. Mater. Struct*., 2019, vol. 42, pp. 2794–2807. https://doi.org/10.1111/ffe.13123
30. Aboulkhair, N.T., Maskery, I., Tuck, C., Ashcroft, I., and Everitt, N.M., Improving the Fatigue Behaviour of a Selectively Laser Melted Aluminium Alloy: Influence of Heat Treatment and Surface Quality, *Mater. Des*., 2016, vol. 104, pp. 174–182. https://doi.org/10.1016/j.matdes.2016.05.041
31. Baek, M.S., Kreethi, R., Park, T.H., Sohn, Y., and Lee, K.A., Influence of Heat Treatment on the High-Cycle Fatigue Properties and Fatigue Damage Mechanism of Selective Laser Melted AlSi10Mg Alloy, *Mater. Sci. Eng. A*, 2021, vol. 819, p. 141486. https://doi.org/10.1016/j.msea.2021.141486
32. Zhang, C., Zhu, H., Liao, H., Cheng, Y., Hu, Z., and Zeng, X., Effect of Heat Treatments on Fatigue Property of Selective Laser Melting AlSi10Mg, *Int. J. Fatigue*, 2018, vol. 116, pp. 513–522. https://doi.org/10.1016/j.ijfatigue.2018.07.016
33. Yu, H., Li, F., Wang, Z., and Zeng, X., Fatigue Performances of Selective Laser Melted Ti-6Al-4V Alloy: Influence of Surface Finishing, Hot Isostatic Pressing and Heat Treatments, *Int. J. Fatigue*, 2019, vol. 120, pp. 175–183. https://doi.org/10.1016/j.ijfatigue.2018.11.019
34. Li, P., Warner, D.H., Pegues, J.W., Roach, M.D., Shamsaei, N., and Phan, N., Investigation of the Mechanisms by Which Hot Isostatic Pressing Improves the Fatigue Performance of Powder Bed Fused Ti-6Al-4V, *Int. J. Fatigue*, 2019, vol. 120, pp. 342–352. https://doi.org/10.1016/j.ijfatigue.2018.10.015
35. Molaei, R., Fatemi, A., and Phan, N., Significance of Hot Isostatic Pressing (HIP) on Multiaxial Deformation and Fatigue Behaviors of Additive Manufactured Ti-6Al-4V Including Build Orientation and Surface Roughness Effects, *Int. J. Fatigue*, 2018, vol. 117,| pp. 352–370. https://doi.org/10.1016/j.ijfatigue.2018.07.035
36. Ertuğrul, O., Öter, Z.Ç., Yılmaz, M.S., Şahin, E., Coşkun, M., Tarakçı, G., and Koç, E., Effect of HIP Process and Subsequent Heat Treatment on Microstructure and Mechanical Properties of Direct Metal Laser Sintered AlSi10Mg Alloy, *Rapid Prototyp. J*., 2020, vol. 26, pp. 1421–1434. https://doi.org/10.1108/RPJ-07-2019-0180
37. Schneller, W., Leitner, M., Springer, S., Grün, F., and Taschauer, M., Effect of Hip Treatment on Microstructure and Fatigue Strength of Selectively Laser Melted AlSi10Mg, *J. Manuf. Mater. Process*, 2019, vol. 3. https://doi.org/10.3390/jmmp3010016
38. Michi, R.A., Plotkowski, A., Shyam, A., Dehoff, R.R., and Babu, S.S., Towards High-Temperature Applications of Aluminium Alloys Enabled by Additive Manufacturing, *Int. Mater. Rev.*, 2022, vol. 67, pp. 298–345. https://doi.org/10.1080/09506608.2021.1951580
39. Zinovieva, O., Romanova, V., Balokhonov, R., and Emelyanova, T., A review of Microstructure and Mechanical Properties of Additively Manufactured Aluminum Alloys, *AIP Conf. Proc*., 2020, vol. 2310. https://doi.org/10.1063/5.0035085
40. Prashanth, K.G., Scudino, S., and Eckert, J., Defining the Tensile Properties of Al-12Si Parts Produced by Selective Laser Melting, *Acta Mater*., 2017, vol. 126, pp. 25–35. https://doi.org/10.1016/j.actamat.2016.12.044
41. Li, P., Kim, Y., Bobel, A.C., Hector, L.G., Sachdev, A.K., Kumar, S., and Bower, A.F., Microstructural Origin of the Anisotropic Flow Stress of Laser Powder Bed Fused AlSi10Mg, *Acta Mater*., 2021, vol. 220. https://doi.org/10.1016/j.actamat.2021.117346
42. Santos Macías, J.G., Douillard, T., Zhao, L., Maire, E., Pyka, G., and Simar, A., Influence on Microstructure, Strength and Ductility of Build Platform Temperature during Laser Powder Bed Fusion of AlSi 10Mg, *Acta Mater*., 2020, vol. 201, pp. 231–243. https://doi.org/10.1016/j.actamat.2020.10.001
43. Liu, Q., Wu, H., Paul, M.J., He, P., Peng, Z., Gludovatz, B., Kruzic, J.J., Wang, C.H., and Li, X., Machine-Learning Assisted Laser Powder Bed Fusion Process Optimization for AlSi10Mg: New Microstructure Description Indices and Fracture Mechanisms, *Acta Mater.*, 2020, vol. 201, pp. 316–328. https://doi.org/10.1016/j.actamat.2020.10.010
44. Xu, Z., Liu, A., and Wang, X., Fatigue Performance and Crack Propagation Behavior of Selective Laser Melted AlSi10Mg in 0°, 15°, 45° and 90° Building

Directions, *Mater. Sci. Eng. A*, 2021, vol. 812, p. 141141. https://doi.org/10.1016/j.msea.2021.141141
45. Paul, M.J., Liu, Q., Best, J.P., Li, X., Kruzic, J.J., Ramamurty, U., and Gludovatz, B., Fracture Resistance of AlSi10Mg Fabricated by Laser Powder Bed Fusion, *Acta Mater*., 2021, vol. 211, p. 116869. https://doi.org/10.1016/j.actamat.2021.116869
46. Giovagnoli, M., Silvi, G., Merlin, M., and Di Giovanni, M.T., Optimisation of Process Parameters for an Additively Manufactured AlSi10Mg Alloy: Limitations of the Energy Density-Based Approach on Porosity and Mechanical Properties Estimation, *Mater. Sci. Eng. A*, 2021, vol. 802, p. 140613. https://doi.org/10.1016/j.msea.2020.140613
47. Aboulkhair, N.T., Everitt, N.M., Ashcroft, I., and Tuck, C., Reducing Porosity in AlSi10Mg Parts Processed by Selective Laser Melting, *Addit. Manuf*., 2014, vol. 1, pp. 77–86. https://doi.org/10.1016/j.addma.2014.08.001
48. Xu, Z.W., Wang, Q., Wang, X.S., Tan, C.H., Guo, M.H., and Gao, P.B., High Cycle Fatigue Performance of AlSi10Mg Alloy Produced by Selective Laser Melting, *Mech. Mater.*, 2020, vol. 148. https://doi.org/10.1016/j.mechmat.2020.103499
49. Tang, M. and Pistorius, P.C., Oxides, Porosity and Fatigue Performance of AlSi10Mg Parts Produced by Selective Laser Melting, *Int. J. Fatigue*, 2017, vol. 94, pp. 192–201. https://doi.org/10.1016/j.ijfatigue.2016.06.002
50. Romano, S., Brückner-Foit, A., Brandão, A., Gumpinger, J., Ghidini, T., and Beretta, S., Fatigue Properties of AlSi10Mg Obtained by Additive Manufacturing: Defect-Based Modelling and Prediction of Fatigue Strength, *Eng. Fract. Mech.*, 2018, vol. 187, pp. 165–189. https://doi.org/10.1016/j.engfracmech.2017.11.002
51. Bao, J., Wu, S., Withers, P.J., Wu, Z., Li, F., Fu, Y., and Sun, W., Defect Evolution during High Temperature Tension-Tension Fatigue of SLM AlSi10Mg Alloy by Synchrotron Tomography, *Mater. Sci. Eng. A*, 2020, vol. 792, p. 139809. https://doi.org/10.1016/j.msea.2020.139809
52. Wu, Z., Wu, S., Bao, J., Qian, W., Karabal, S., Sun, W., and Withers, P.J., The Effect of Defect Population on the Anisotropic Fatigue Resistance of AlSi10Mg Alloy Fabricated by Laser Powder Bed Fusion, *Int. J. Fatigue*, 2021, vol. 151, p. 106317. https://doi.org/10.1016/j.ijfatigue.2021.106317
53. Romano, S., Abel, A., Gumpinger, J., Brandão, A.D., and Beretta, S., Quality Control of AlSi10Mg Produced by SLM: Metallography Versus CT Scans for Critical Defect Size Assessment, *Addit. Manuf*., 2019, vol. 28, pp. 394–405. https://doi.org/10.1016/j.addma.2019.05.017
54. Biswal, R., Zhang, X., Shamir, M., Al Mamun, A., Awd, M., Walther, F., and Khadar Syed, A., Interrupted Fatigue Testing with Periodic Tomography to Monitor Porosity Defects in Wire + Arc Additive Manufactured Ti-6Al-4V, *Addit. Manuf*., 2019, vol. 28, pp. 517–527. https://doi.org/10.1016/j.addma.2019.04.026
55. Qian, W., Wu, S., Wu, Z., Ahmed, S., Zhang, W., Qian, G., and Withers, P.J., In Situ X-Ray Imaging of Fatigue Crack Growth From Multiple Defects In Additively Manufactured AlSi10Mg Alloy, *Int. J. Fatigue*, 2022, vol. 155, p. 106616. https://doi.org/10.1016/j.ijfatigue.2021.106616
56. Piscopo, G., Atzeni, E., Calignano, F., Galati, M., Iuliano, L., Minetola, P., and Salmi, A., Machining Induced Residual Stresses in AlSi10Mg Component Produced by Laser Powder Bed Fusion (L-PBF), *Proc. CIRP*, 2019, vol. 79, pp. 101–106. https://doi.org/10.1016/j.procir.2019.02.019
57. Wu, J., Wang, L., and An, X., Numerical Analysis of Residual Stress Evolution of AlSi10Mg Manufactured by Selective Laser Melting, *Optik (Stuttg.)*, 2017, vol. 137, pp. 65–78. https://doi.org/10.1016/j.ijleo.2017.02.060
58. Sahoo, S., Direct Metal Laser Sintering of AlSi10Mg Alloy Parts: Modeling of Temperature Profile, *Mater. Today Proc*., 2021, vol. 35, pp. 118–123. https://doi.org/10.1016/j.matpr.2020.03.342
59. Marola, S., Bosia, S., Veltro, A., Fiore, G., Manfredi, D., Lombardi, M., Amato, G., Baricco, M., and Battezzati, L., Residual Stresses in Additively Manufactured AlSi10Mg: Raman Spectroscopy and X-Ray Diffraction Analysis, *Mater. Des.*, 2021, vol. 202, p. 109550. https://doi.org/10.1016/j.matdes.2021.109550
60. Samantaray, M., Sahoo, S., and Thatoi, D., Computational Modeling of Heat Transfer and Sintering Behavior during Direct Metal Laser Sintering of AlSi10Mg Alloy Powder, *Comptes Rendus Mec.*, 2018, vol. 346, pp. 1043–1054. https://doi.org/10.1016/j.crme.2018.08.006
61. Chen, S., Gao, H., Zhang, Y., Wu, Q., Gao, Z., and Zhou, X., Review on Residual Stresses in Metal Additive Manufacturing: Formation Mechanisms, Parameter Dependencies, Prediction and Control Approaches, *J. Mater. Res. Technol*., 2022, vol. 17, pp. 2950–2974. https://doi.org/10.1016/j.jmrt.2022.02.054
62. Salmi, A., Atzeni, E., Iuliano, L., and Galati, M., Experimental Analysis of Residual Stresses on AlSi10Mg Parts Produced by Means of Selective Laser Melting (SLM), *Proc. CIRP*, 2017, vol. 62, pp. 458–463. https://doi.org/10.1016/j.procir.2016.06.030
63. Beretta, S., Gargourimotlagh, M., Foletti, S., du Plessis, A., and Riccio, M., Fatigue Strength Assessment of "as Built" AlSi10Mg Manufactured by SLM with Different Build Orientations, *Int. J. Fatigue*, 2020, vol. 139, p. 105737. https://doi.org/10.1016/j.ijfatigue.2020.105737
64. Panda, B.K. and Sahoo, S., Thermo-Mechanical Modeling and Validation of Stress Field during Laser Powder Bed Fusion of AlSi10Mg Built Part, *Results*

Phys., 2019, vol. 12, pp. 1372–1381. https://doi.org/10.1016/j.rinp.2019.01.002

65. Rasul Nazami, G., Kalyan Panda, B., and Sahoo, S., Finite Element Simulation of Residual Stress in Direct Metal Laser Sintering of AlSi10Mg Built Part: Effect of Laser Spot Overlapping, *Mater. Today Proc*., 2021, vol. 41, pp. 445–450. https://doi.org/10.1016/j.matpr.2020.09.844
66. Awd, M., Siddique, S., Johannsen, J., Emmelmann, C., and Walther, F., Very High-Cycle Fatigue Properties and Microstructural Damage Mechanisms of Selective Laser Melted AlSi10Mg Alloy, *Int. J. Fatigue*, 2019, vol. 124, pp. 55–69. https://doi.org/10.1016/j.ijfatigue.2019.02.040
67. Tridello, A., Fiocchi, J., Biffi, C.A., Rossetto, M., Tuissi, A., and Paolino, D.S., Size-Effects Affecting the Fatigue Response up to 10^9 Cycles (VHCF) of SLM AlSi10Mg Specimens Produced in Horizontal and Vertical Directions, *Int. J. Fatigue*, 2022, vol. 160, p. 106825. https://doi.org/10.1016/j.ijfatigue.2022.106825
68. Tridello, A., Biffi, C.A., Fiocchi, J., Bassani, P., Chiandussi, G., Rossetto, M., Tuissi, A., and Paolino, D.S., VHCF Response of As-Built SLM AlSi10Mg Specimens with Large Loaded Volume, *Fatigue Fract. Eng. Mater. Struct*., 2018, vol. 41, pp. 1918–1928. https://doi.org/10.1111/ffe.12830
69. Tridello, A., Niutta, C.B., Berto, F., and Paolino, D.S., Size-Effect in Very High Cycle Fatigue: A Review, *Int. J. Fatigue*, 2021, vol. 153, p. 106462. https://doi.org/10.1016/j.ijfatigue.2021.106462
70. Paolino, D.S., Tridello, A., Fiocchi, J., Biffi, C.A., Chiandussi, G., Rossetto, M., and Tuissi, A., VHCF Response up to 109 Cycles of SLM AlSi10Mg Specimens Built in a Vertical Direction, *Appl. Sci.*, 2019, vol. 9. https://doi.org/10.3390/app9152954
71. Yang, T., Liu, T., Liao, W., MacDonald, E., Wei, H., Chen, X., and Jiang, L., The Influence of Process Parameters on Vertical Surface Roughness of the AlSi10Mg Parts Fabricated by Selective Laser Melting, *J. Mater. Process. Technol*., 2019, vol. 266, pp. 26–36. https://doi.org/10.1016/j.jmatprotec.2018.10.015
72. Maamoun, A.H., Xue, Y.F., Elbestawi, M.A., and Veldhuis, S.C., Effect of Selective Laser Melting Process Parameters on the Quality of Al Alloy Parts: Powder Characterization, Density, Surface Roughness, and Dimensional Accuracy, *Materials (Basel)*, 2018, vol. 11. https://doi.org/10.3390/ma11122343
73. Pegues, J., Roach, M., Scott Williamson, R., and Shamsaei, N., Surface Roughness Effects on the Fatigue Strength of Additively Manufactured Ti-6Al-4V, *Int. J. Fatigue*, 2018, vol. 116, pp. 543–552. https://doi.org/10.1016/j.ijfatigue.2018.07.013
74. Bagehorn, S., Wehr, J., and Maier, H.J., Application of Mechanical Surface Finishing Processes for Roughness Reduction and Fatigue Improvement of Additively Manufactured Ti-6Al-4V Parts, *Int. J. Fatigue*, 2017, vol. 102, pp. 135–142. https://doi.org/10.1016/j.ijfatigue.2017.05.008
75. Uzan, N.E., Shneck, R., Yeheskel, O., and Frage, N., Fatigue of AlSi10Mg Specimens Fabricated by Additive Manufacturing Selective Laser Melting (AM-SLM), *Mater. Sci. Eng. A*, 2017, vol. 704, pp. 229–237. https://doi.org/10.1016/j.msea.2017.08.027
76. Nicoletto, G., Gallina, L., and Riva, E., Influence of As-Built Surfaces on the Fatigue Behavior of AlSi10Mg Parts Obtained by Laser Powder Bed Fusion, *Proc. Struct. Integr*., 2019, vol. 24, pp. 381–389. https://doi.org/10.1016/j.prostr.2020.02.035
77. Chang, S., Liu, A., Ong, C.Y.A., Zhang, L., Huang, X., Tan, Y.H., Zhao, L., Li, L., and Ding, J., Highly Effective Smoothening of 3D-Printed Metal Structures Via Overpotential Electrochemical Polishing, *Mater. Res. Lett*., 2019, vol. 7, pp. 282–289. https://doi.org/10.1080/21663831.2019.1601645
78. Avanzini, A., Battini, D., Gelfi, M., Girelli, L., Petrogalli, C., Pola, A., and Tocci, M., Investigation on Fatigue Strength of Sand-Blasted DMLS-AlSi10Mg Alloy, *Proc. Struct. Integr*., 2019, vol. 18, pp. 119–128. https://doi.org/10.1016/j.prostr.2019.08.146
79. Sagbas, B., Post-Processing Effects on Surface Properties of Direct Metal Laser Sintered AlSi10Mg Parts, *Met. Mater. Int*., 2020, vol. 26, pp. 143–153. https://doi.org/10.1007/s12540-019-00375-3
80. Damon, J., Dietrich, S., Vollert, F., Gibmeier, J., and Schulze, V., Process Dependent Porosity and the Influence of Shot Peening on Porosity Morphology Regarding Selective Laser Melted AlSi10Mg Parts, *Addit. Manuf*., 2018, vol. 20, pp. 77–89. https://doi.org/10.1016/j.addma.2018.01.001
81. Du Plessis, A., Glaser, D., Moller, H., Mathe, N., Tshabalala, L., Mfusi, B., and Mostert, R., Pore Closure Effect of Laser Shock Peening of Additively Manufactured AlSi10Mg, *3D Print. Addit. Manuf*., 2019, vol. 6, pp. 245–252. https://doi.org/10.1089/3dp.2019.0064
82. Kalentics, N., de Seijas, M.O.V., Griffiths, S., Leinenbach, C., and Logé, R.E., 3D Laser Shock Peening—A New Method for Improving Fatigue Properties of Selective Laser Melted Parts, *Addit. Manuf*., 2020, vol. 33, p. 101112. https://doi.org/10.1016/j.addma.2020.101112
83. Li, J., Sun, J., Qian, G., and Shi, L., Defect-Induced Cracking and Fine Granular Characteristics in Very-High-Cycle Fatigue of Laser Powder Bed Fusion AlSi 10Mg Alloy, *Int. J. Fatigue*, 2022, vol. 158, p. 106770. https://doi.org/10.1016/j.ijfatigue.2022.106770
84. Du, L., Pan, X., Qian, G., Zheng, L., and Hong, Y., Crack Initiation Mechanisms under Two Stress Ratios up to Very-High-Cycle Fatigue Regime for a Selective Laser Melted Ti-6Al-4V, *Int. J. Fatigue*, 2021, vol. 149, p. 106294. https://doi.org/10.1016/j.ijfatigue.2021.106294

85. Fu, R., Zheng, L., Ling, C., Zhong, Z., and Hong, Y., An Experimental Investigation of Fatigue Performance and Crack Initiation Characteristics for an SLMed Ti-6Al-4V under Different Stress Ratios up to Very-High-Cycle Regime, *Int. J. Fatigue*, 2022, vol. 164, p. 107119. https://doi.org/10.1016/j.ijfatigue.2022.107119
86. Hong, Y., Liu, X., Lei, Z., and Sun, C., The Formation Mechanism of Characteristic Region at Crack Initiation for Very-High-Cycle Fatigue of High-Strength Steels, *Int. J. Fatigue*, 2016, vol. 89, pp. 108–118. https://doi.org/10.1016/j.ijfatigue.2015.11.029
87. Beevers, E., Brandão, A.D., Gumpinger, J., Gschweitl, M., Seyfert, C., Hofbauer, P., Rohr, T., and Ghidini, T., Fatigue Properties and Material Characteristics of Additively Manufactured AlSi10Mg—Effect of the Contour Parameter on the Microstructure, Density, Residual Stress, Roughness and Mechanical Properties, *Int. J. Fatigue*, 2018, vol. 117, pp. 148–162. https://doi.org/10.1016/j.ijfatigue.2018.08.023
88. Tridello, A., Fiocchi, J., Biffi, C.A., Chiandussi, G., Rossetto, M., Tuissi, A., and Paolino, D.S., Effect of Microstructure, Residual Stresses and Building Orientation on the Fatigue Response up to 10^9 Cycles of an SLM AlSi10Mg Alloy, *Int. J. Fatigue*, 2020, vol. 137, p. 105659. https://doi.org/10.1016/j.ijfatigue.2020.105659
89. Roveda, I., Serrano-Munoz, I., Kromm, A., and Madia, M., Investigation of Residual Stresses and Microstructure Effects on the Fatigue Behaviour of a L-PBF AlSi10Mg Alloy, *Proc. Struct. Integr*., 2021, vol. 38, pp. 564–571. https://doi.org/10.1016/j.prostr.2022.03.057
90. Guo, M., Ye, Y., Jiang, X., and Wang, L., Microstructure, Mechanical Properties and Residual Stress of Selective Laser Melted AlSi10Mg, *J. Mater. Eng. Perform*., 2019, vol. 28, pp. 6753–6760. https://doi.org/10.1007/s11665-019-04423-2
91. Ardi, D.T., Guowei, L., Maharjan, N., Mutiargo, B., Leng, S.H., and Srinivasan, R., Effects of Post-Processing Route on Fatigue Performance of Laser Powder Bed Fusion Inconel 718, *Addit. Manuf*, 2020, vol. 36, p. 101442. https://doi.org/10.1016/j.addma.2020.101442
92. Yu, C., Huang, Z., Zhang, Z., Wang, J., Shen, J., and Xu, Z., Effects of Sandblasting and HIP on Very High Cycle Fatigue Performance of SLM-Fabricated IN718 Superalloy, *J. Mater. Res. Technol*., 2022, vol. 18, pp. 29–43. https://doi.org/10.1016/j.jmrt.2022.02.077
93. Hirata, T., Kimura, T., and Nakamoto, T., Effects of Hot Isostatic Pressing and Internal Porosity on the Performance of Selective Laser Melted AlSi10Mg Alloys, *Mater. Sci. Eng. A*, 2020, vol. 772, p. 138713. https://doi.org/10.1016/j.msea.2019.138713
94. Araújo, L.C., Gabriel, A.H.G., da Fonseca, E.B., Avila, J.A., Jardini, A.L., Seno Junior, R., and Lopes, É.S.N., Effects of Build Orientation and Heat Treatments on the Tensile and Fracture Toughness Properties of Additively Manufactured AlSi10Mg, *Int. J. Mech. Sci*., 2022, vol. 213. https://doi.org/10.1016/j.ijmecsci.2021.106868
95. Muro-Barrios, R., Cui, Y., Lambros, J., and Chew, H.B., Dual-Scale Porosity Effects on Crack Growth in Additively Manufactured Metals: 3D Ductile Fracture Models, *J. Mech. Phys. Solids*, 2022, vol. 159, p. 104727. https://doi.org/10.1016/j.jmps.2021.104727
96. Jamshidian, M., Promoppatum, P., Ramamurty, U., and Jhon, M.H., Modulating Fracture Toughness through Processing-Mediated Mesostructure in Additively Manufactured Al-12Si Alloy, *Mater. Des*., 2022, vol. 215, p. 110440. https://doi.org/10.1016/j.matdes.2022.110440
97. Murakami, Y. and Endo, M., Effects of Defects, Inclusions and Inhomogeneities on Fatigue Strength, *Int. J. Fatigue*, 1994, vol. 16, pp. 163–182. https://doi.org/10.1016/0142-1123(94)90001-9
98. Romano, S., Brandão, A., Gumpinger, J., Gschweitl, M., and Beretta, S., Qualification of AM Parts: Extreme Value Statistics Applied to Tomographic Measurements, *Mater. Des*., 2017, vol. 131, pp. 32–48. https://doi.org/10.1016/j.matdes.2017.05.091
99. Hu, Y.N., Wu, S.C., Wu, Z.K., Zhong, X.L., Ahmed, S., Karabal, S., Xiao, X.H., Zhang, H.O., and Withers, P.J., A New Approach to Correlate the Defect Population with the Fatigue Life of Selective Laser Melted Ti-6Al-4V Alloy, *Int. J. Fatigue*, 2020, vol. 136. https://doi.org/10.1016/j.ijfatigue.2020.105584
100. Masuo, H., Tanaka, Y., Morokoshi, S., Yagura, H., Uchida, T., Yamamoto, Y., and Murakami, Y., Influence of Defects, Surface Roughness and HIP on the Fatigue Strength of Ti-6Al-4V Manufactured by Additive Manufacturing, *Int. J. Fatigue*, 2018, vol. 117, pp. 163–179. https://doi.org/10.1016/j.ijfatigue.2018.07.020
101. Wang, Q.Y., Berard, J.Y., Dubarre, A., Baudry, A., Rathery, S., and Bathias, C., Gigacycle Fatigue of Ferrous Alloys, *Fatigue Fract. Eng. Mater. Struct.*, 1999, vol. 22, pp. 667–672. https://doi.org/10.1046/j.1460-2695.1999.00185.x
102. Zhang, Y., Li, X., Yuan, S., Sun, R., Sakai, T., Lashari, M.I., Hamid, U., and Li, W., High-Cycle-Fatigue Properties of Selective-Laser-Melted AlSi10Mg with Multiple Building Directions, *Int. J. Mech. Sci.*, 2022, vol. 224, p. 107336. https://doi.org/10.1016/j.ijmecsci.2022.107336
103. Kitagawa, H. and Takahashi, S., Applicability of Fracture Mechanics to Very Small Cracks or the Cracks in the Early Stage, in *Proc 2nd Int. Conf. Mech. Behav. Mater. ICM2*, 1976, pp. 627–631.
104. Zerbst, U., Madia, M., Vormwald, M., and Beier, H.T., Fatigue Strength and Fracture Mechanics—A General Perspective, *Eng. Fract. Mech.*, 2018,

vol. 198, pp. 2–23. https://doi.org/10.1016/j.engfracmech.2017.04.030
105. Beretta, S. and Romano, S., A Comparison of Fatigue Strength Sensitivity to Defects for Materials Manufactured by AM or Traditional Processes, *Int. J. Fatigue*, 2017, vol. 94, pp. 178–191. https://doi.org/10.1016/j.ijfatigue.2016.06.020
106. Greitemeier, D., Dalle Donne, C., Syassen, F., Eufinger, J., and Melz, T., Effect of Surface Roughness on Fatigue Performance of Additive Manufactured Ti–6Al–4V, *Mater. Sci. Technol*., 2016, vol. 32, pp. 629–634. https://doi.org/10.1179/1743284715Y.0000000053
107. Yadollahi, A., Mahtabi, M.J., Khalili, A., Doude, H.R., and Newman, J.C., Fatigue Life Prediction of Additively Manufactured Material: Effects of Surface Roughness, Defect Size, and Shape, *Fatigue Fract. Eng. Mater. Struct*., 2018, vol. 41, pp. 1602–1614. https://doi.org/10.1111/ffe.12799
108. Yadollahi, A., Mahmoudi, M., Elwany, A., Doude, H., Bian, L., and Newman, J.C., Fatigue-Life Prediction of Additively Manufactured Material: Effects of Heat Treatment and Build Orientation, *Fatigue Fract. Eng. Mater. Struct*., 2020, vol. 43, pp. 831–844. https://doi.org/10.1111/ffe.13200
109. Tanaka, K. and Mura, T., A Theory of Fatigue Crack Initiation at Inclusions, *Metall. Trans. A*, 1982, vol. 13, pp. 117–123. https://doi.org/10.1007/BF02642422
110. Nadot, Y., Nadot-Martin, C., Kan, W.H., Boufadene, S., Foley, M., Cairney, J., Proust, G., and Ridosz, L., Predicting the Fatigue Life of an AlSi10Mg Alloy Manufactured Via Laser Powder Bed Fusion by Using Data from Computed Tomography, *Addit. Manuf*., 2020, vol. 32, p. 100899. https://doi.org/10.1016/j.addma.2019.100899
111. Zhang, W., Hu, Y., Ma, X., Qian, G., Zhang, J., Yang, Z., and Berto, F., Very-High-Cycle Fatigue Behavior of AlSi10Mg Manufactured by Selected Laser Melting: Crystal Plasticity Modeling, *Int. J. Fatigue*, 2021, vol. 145, p. 106109. https://doi.org/10.1016/j.ijfatigue.2020.106109
112. Zhang, J., Li, J., Wu, S., Zhang, W., Sun, J., and Qian, G., High-Cycle and Very-High-Cycle Fatigue Lifetime Prediction of Additively Manufactured AlSi10Mg via Crystal Plasticity Finite Element Method, *Int. J. Fatigue*, 2022, vol. 155, p. 106577. https://doi.org/10.1016/j.ijfatigue.2021.106577
113. Zhan, Z., Hu, W., and Meng, Q., Data-Driven Fatigue Life Prediction in Additive Manufactured Titanium Alloy: A Damage Mechanics Based Machine Learning Framework, *Eng. Fract. Mech*., 2021, vol. 252, p. 107850. https://doi.org/10.1016/j.engfracmech.2021.107850
114. Li, J., Yang, Z., Qian, G., and Berto, F., Machine Learning Based Very-High-Cycle Fatigue Life Prediction of Ti-6Al-4V Alloy Fabricated by Selective Laser Melting, *Int. J. Fatigue*, 2022, vol. 158, p. 106764. https://doi.org/10.1016/j.ijfatigue.2022.106764
115. Maleki, E., Bagherifard, S., Razavi, S.M.J., Bandini, M., du Plessis, A., Berto, F., and Guagliano, M., On the Efficiency of Machine Learning for Fatigue Assessment of Post-Processed Additively Manufactured AlSi10Mg, *Int. J. Fatigue*, 2022, vol. 160, p. 106841. https://doi.org/10.1016/j.ijfatigue.2022.106841
116. Zhang, M., Sun, C.N., Zhang, X., Goh, P.C., Wei, J., Hardacre, D., and Li, H., High Cycle Fatigue Life Prediction of Laser Additive Manufactured Stainless Steel: A Machine Learning Approach, *Int. J. Fatigue*, 2019, vol. 128, p. 105194. https://doi.org/10.1016/j.ijfatigue.2019.105194
117. Zhan, Z. and Li, H., A Novel Approach Based on the Elastoplastic Fatigue Damage and Machine Learning Models for Life Prediction of Aerospace Alloy Parts Fabricated by Additive Manufacturing, *Int. J. Fatigue*, 2021, vol. 145, p. 106089. https://doi.org/10.1016/j.ijfatigue.2020.106089